Effect of Carbon Sources and Carbonaceous Atmospheres on the Effective Synthesis of Nanostructured Tungsten Carbide Powders

by

Philipp Hoier

Diploma work No. 141/2014

at Department of Materials and Manufacturing Technology

CHALMERS UNIVERSITY OF TECHNOLOGY

Gothenburg, Sweden

Diploma work in the Master programme Materials Engineering

Performed at: Department of Materials and Manufacturing Technology

Chalmers University of Technology, SE - 412 96 Gothenburg

Supervisor   :   Dr. Raquel De Oro Calderón

Department of Materials and Manufacturing Technology

Chalmers University of Technology, SE - 412 96 Gothenburg

Examiner &

Co-Supervisor: Assoc. Prof. Eduard Hryha

Department of Materials and Manufacturing Technology

Chalmers University of Technology, SE - 412 96 Gothenburg

Effect of Carbon Sources and Carbonaceous Atmospheres on the Effective Synthesis of Nanostructured Tungsten Carbide Powders

Effect of Carbon Sources and Carbonaceous Atmospheres on the Effective Synthesis of Nanostructured Tungsten Carbide Powders

Philipp Hoier

Department of Materials and Manufacturing Technology
Chalmers University of Technology

Abstract

Owing to its ultra-fine microstructure, nanostructured tungsten carbide (WC) powders characterized by advanced mechanical properties are of highest interest for the metal cutting industry where they are used for the production of cemented carbide cutting tools. In this work, WC synthesis from precursor mixes containing tungsten powder (in form of W or WO_3 powder) and carbon sources (as graphite or carbon black) is achieved by a two-step process. Mechanical activation by ball milling of the precursor powders is followed by thermal activation at 1100 °C for 30 min in Ar or Ar-10%CO atmospheres. Depending on the tungsten source (W or WO_3 powder) solid carbon provides either solely carburization, or both reduction and carburization, which can be assisted by the presence of CO in the synthesis atmosphere.

The results show that homogeneous, fine mixes of the base powders after milling offer large contact area and improve reactivity between the precursors. Synthesis of pure WC powders is achieved at 1100 ^{0}C in inert Ar atmosphere when using metallic tungsten as precursor. Using oxide precursors (WO_3), synthesis is not completed at 1100 ^{0}C in Ar atmosphere, however, a significant improvement in the efficiency of the synthesis is achieved when using Ar-10%CO atmospheres. Although the reducing activity of CO seems to be low in the conditions studied in this work, improved carburization of metallic tungsten by CO might be the key for improving efficiency of the synthesis process.

Table of Contents

1 Introduction

1.1 Hard Metals and Cemented Carbides

Tungsten carbides (WC) as other carbides of the transition metals (e.g. TiC, TaC) find extensive application as tool materials and wear resistant components. This is owing to their high hardness and strength. Combining it with a tough and ductile metallic binder offers a composite suitable for tool materials used in e.g. metal cutting inserts and mining tools [1].

Specifically the largest portion of WC is used as cemented carbides in combination with Co as the matrix phase. Unalloyed cemented carbides consist of only two phases, WC (α-phase) and Co (β-phase) and are referred to as straight grades. Their mechanical properties such as hardness, transverse rupture strength and fracture toughness are tailored by the WC grain size as well as the Co binder content. Commonly the range of carbide content is 70 to 97 wt.% while the WC grain size is between 0.2 and 14 μm. Alloying of Co by e.g. Ni, Cr or using other corrosion resistant alloys as the binder phase can improve the corrosion resistance. Moreover addition of other carbides as TiC, TaC or NbC (γ-phase) is done in order to improve high temperature properties, especially relevant in metal cutting. These are referred to as "metal grades" or "mixed grades" [2].

Cemented carbides are manufactured by means of powder metallurgy. According to the desired properties, a specific powder mix is prepared by milling. This mix contains powders of WC (sometimes also other carbides), the binder metal as well as process aids as lubricants in the exact right proportions. Granulation processes can be applied in order to increase the flow and fill properties of the obtained powder for the consecutive pressing operation. Granulated powder particles are weakly bonded agglomerates – ideally spherical – of very fine carbide particles. The mixing and granulation is followed by powder consolidation techniques such as direct compacting, cold isostatic pressing or extrusion, which give a near net shape green body with about 60 % of the theoretical attainable density. [3] After thermal removal of the lubricants, sintering at about 1600 – 1800 K (depending on eutectic temperature of the cobalt phase) is carried out during which the compact undergoes shrinkage and gains density. Throughout the process cobalt melts, individual carbide particles join together and are wetted by the liquid cobalt. Some of the WC dissolves in the liquid cobalt phase and grain growth occurs as the carbides precipitate. Generally the sintering process is accompanied by a carbide grain size increase. The finer grain size the higher the performance in service. There are ways of preserving the fine grain structure throughout sintering such as the use of grain growth inhibitors like vanadium, tantalum, and chromium carbides [4].

The global annual consumption of tungsten in 2010 was estimated to be 95000 t. In Europe the vast majority of 72 % was used in form of tungsten carbide in cemented carbides [5]. The biggest share of worldwide cemented carbide turnover can be assigned to the field of machining. This is due to the fact that cemented carbide inserts are used in a very broad field of machining operations such as turning, boring or drilling of e.g. metals, wood, polymers and composites [6]. It is estimated that about 70-90 % of all used metal cutting inserts are based on Cemented Carbides [7]. This shows the important role that tungsten carbide plays in the field of machining which represents probably the most common manufacturing process of products. It is therefore crucial to find new ways of further improving cemented carbide properties.

1.2   Properties of Nanocrystalline Cemented Carbides

Decreasing grain size increases the hardness of polycrystalline metals. This phenomena is described by the Hall-Petch relation [7,8]:

$$\sigma_y = \sigma_0 + k_y d^{-1/2}$$

Where d is the average grain diameter, k_y and σ_0 are material parameters for the stress required to start dislocation movement and the strengthening coefficient, respectively. In case of fine grained tungsten carbide the hardness is in the range of 2400 – 2800 kg·mm^{-2} (HV30) [10]. It has been shown that a decrease in WC grain size increases wear resistance as well as hardness, compression and bending strength of different WC-Co hardmetals [11][12]. Table 1 summarizes the positive effect of finer WC grain size on the mechanical properties of a specific hardmetal for two different grain size ranges.

Table 1: Effect of WC grain size on mechanical properties of 90WC-10Co hardmetal [11]**.**

Property	Fine WC	Coarse WC
Grain size [µm]	0.5 – 1.0	2.0 – 5.0
Rockwell hardness [HRA]	90.7 – 91.3	87.4 – 88.2
Bending strength [MPa]	3100	2760
Compression strength [MPa]	5170	4000
Young modulus [GPa]	620	552
Relative wear resistance	22	7

Based on previously shown results further decrease in WC grain size is highly promising in improving the performance of WC-Co hardmetals. Studies have also shown that decreasing WC particle size lowers the necessary WC-Co sintering temperature to get the required densification. The lower temperature in turn helps avoiding WC grain growth and retaining the initial nano-crystallinity throughout the sintering [13][14].
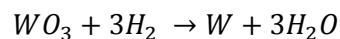
1.3   Production of WC Powders

1.3.1   Industrial Tungsten Carbide Powder Production

The biggest share of industrially produced tungsten carbide powder is synthesized by carburization of tungsten powder. Therefore high purity tungsten powders with the desired properties have to be produced first. Details on the two processes regarding chemical reactions and critical parameters are given below.
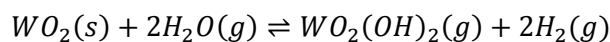
Production of Pure Tungsten Powder – Reduction of Tungsten Oxide by Hydrogen

Pure tungsten powder is most commonly obtained by a reduction process of yellow tungsten oxide (WO$_3$) in flowing hydrogen atmosphere at 600 – 1100 °C. The overall chemical reaction can be described as [10]:
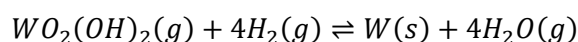
$$WO_3 + 3H_2 \rightarrow W + 3H_2O$$

However, during the process the oxide undergoes different transitions to lower oxides until it eventually forms pure tungsten. Several sequences depending on the process parameters have been

proven [15]. The reduction process at lower temperatures (<750 °C) is based on diffusion and removal of oxygen in the solid state from the oxide particles. The resulting polycrystalline metal particle has a porous sponge-like appearance. Reduction via chemical vapor transport (CVT) happens due to the formation of a volatile tungsten oxide hydrate $WO_2(OH)_2$ from tungsten oxide in the presence of water vapor:

$$WO_2(s) + 2H_2O(g) \rightleftharpoons WO_2(OH)_2(g) + 2H_2(g)$$

Tungsten oxide hydrate then diffuses to tungsten metal surface where it is reduced:

$$WO_2(OH)_2(g) + 4H_2(g) \rightleftharpoons W(s) + 4H_2O(g)$$

Water vapor formation followed by retardation of its diffusion through the powder bed can cause variations in the local atmosphere composition (local humidity), especially in the case of the big batches on industrial scale where large and densely packed powder beds. Local increase in water vapor content stabilizes the oxides and therefore slows down the reaction rate. Humidity also influences the nucleation rate in such a way that the higher the humidity the lower the nucleation rate and subsequently the larger the average grain size. As a consequence of the above described reduction mechanisms, industrial production of very fine grained tungsten powder faces several challenges. To prevent growth of big grains during the reduction, following parameters have to be fulfilled [10]:

- Hydrogen flow in large excess
- Very dry hydrogen
- Small height of powder layer
- High porosity of powder bed
- Low oxide feed
- Low temperature

Especially the high hydrogen flow rates, along with high demands on purity, raise the costs and are drawbacks of this reduction step.

Carburization of Tungsten Powder by Carbon

Conventional tungsten carbide powder production starts from a mix of tungsten powder and carbon. Most commonly carbon black or soot is used as the source of carbon. Thorough blending by means of V-blenders, double cone blenders or ball mills is followed by charging graphite vessels with the tungsten/carbon blends. They are then passed through a furnace at 1300 - 1700 °C in hydrogen atmosphere. After a heat-treatment for one to two hours the vessels are pushed through a cooling zone where it is crucial to avoid contact of powder with the air and moisture. Subsequent milling is done to eliminate particle agglomerates which are formed due to local sintering at high temperatures [16].

The exact mechanisms occurring during carburization are not fully understood, however, it is suggested that only the carbon in close vicinity of tungsten particles can react with tungsten. Carbon further away has to either diffuse (slow process) or be transported by chemical vapor transport (CVT). CVT occurs due to the reaction of hydrogen with solid carbon to form methane CH_4. Methane subsequently moves over larger distances towards tungsten particles where carbon is dissociated (cracked) and can diffuse into the solid particle via a vacancy mechanism [10][17]. Firstly, WC is formed in the outermost layer of the particle [18]. Subsequent carbide formation is limited by the diffusion through the previously formed WC layer (carbon has higher diffusion coefficient in W_2C as compared to WC). While the WC thickness remains constant due to the slower carbon diffusion

through it, carbon diffusion results in the built-up of a W_2C layer growing in radial direction. Only when the entire particle consists of W_2C, the WC layer starts growing and eventually the whole particle will transform to WC [10].

The stoichiometric carbon content in WC is 6.13 wt.-%. However, the amount of carbon needed for the process depends on several factors such as e.g. the particle size of the starting tungsten powder. Smaller particles are characterized by a higher overall content of oxide unavoidably formed on the particles surfaces. These oxides will be reduced by carbon and therefore an increase of required carbon has to be taken into account when processing finer tungsten starting powders. Another factor is the moisture content in the hydrogen [16]. The required furnace temperature for carburization of tungsten depends on the starting materials' particle size. The rate of carburization is inversely proportional to the particle size [19]. Smaller particles mean a shorter diffusion path and subsequently a lower temperature is sufficient for tungsten carbide formation as compared to coarse powder particles [18]. The carburization process is also influenced by the properties of the carbon black or graphite powder admixed to the tungsten powder. Finer carbon particles are generally capable of forming a denser layer on top of tungsten particles which is beneficial in terms of reactivity [10].

1.3.2 Alternative Methods of Nanocrystalline Tungsten Carbide Production

Research efforts have been made in finding novel methods of tungsten carbide production. Both making a direct carburization from the oxide possible and obtaining powders with finer crystal structure in the nanometer range are the main topics of interest. Avoiding the expensive (due to the high hydrogen gas consumption) tungsten oxide reduction step and improved mechanical properties by the nanosized crystalline structure are the driving forces for the research. Table 2 shows an overview of the papers published on the direct production of nanocrystalline WC powders from WO_3 as the starting material. Various carbon sources and reducing atmospheres have been investigated. There is general agreement on the fact that the direct carburization is advantageous in producing fine grained WC powders.

Table 2: Literature review of research focused on nanocrystalline WC powders with summary of relevant investigated aspects of synthesis.

Tungsten Source	Carbon Source	Mixing/Milling Conditions	Thermal Activation	WC Crystalline grain size	Characteristics	Ref
WO$_3$	Graphite (99.99% Aldrich)	WO$_3$, C and Co$_3$O$_4$ Attritor ball mill, WC-balls φ~5mm, 60:1, Ar, 600rpm, 6h	Reduction: 570, 620 or 670 °C for 2 h in Ar-50%H$_2$ Carburization: 1000 °C for 1 h in Ar or CO	40-50nm	- Full reduction WO$_3$→W in Ar-50H$_2$ is completed at 570˚C. Carburization is achieved at 900 ˚C - Formation of WC proceeds with the formation of intermetallics (Co$_3$W, Co$_6$W$_6$C) - Size of WC primary particles 50-700nm - Grain growth at temperatures above 900 ˚C, particularly obvious at 1000 ˚C due to anisotropic crystal growth (truncated triangular prisms and nanoplates)	[20]
			Reduction+Carburization: 900˚C in CO for 2h	30-40nm		
WO$_3$ (99.9 %)	Graphite (>99%)	Planetary ball mill, WC-balls and vial, 10:1, Ar, 350rpm, 10h (8.161 --> 18.582 m2/g or d$_{50}$ change of 574.3 nm to 169.0 nm)	Reduction+Carburization: 740 or 1215˚C in vacuum for 1h	104.7 nm	- At 740 ˚C Main phases W$_{18}$O$_{49}$ and WO$_2$, minor amounts of WO$_3$ and W in un-milled powder - increased reactivity for milled samples: Full WC conversion at 1215 °C - WC formation via intermediate Magneli phases - WC formation from Magneli phases easier for T>727 °C as compared from W (includes thermodynamic analysis)	[21]
WO$_3$ (99.5%)	Carbon black (99.5%)	WO$_3$, C and Co$_3$O$_4$ Planetary ball mill, WC-balls and vial, 3:1, Ethanol, 500rpm, 20h	Reduction+Carburization: 850-1050˚C in vacuum for 4h	-	- Reduction of tungsten and cobalt oxides at 723 – 1173 K - Carburization to WC and W$_2$C at 1123 – 1500 K - Pure WC-Co composite powders with homogeneous and ultrafine particles (300 nm) at 1323 K in vacuum (includes thermodynamic analysis)	[22]
WO$_3$ (5 m^2/g)	Carbon black (246 m^2/g) (20 nm)	Coating of WO3 with C by propylene cracking, Mixing with carbon black	Reduction+Carburization: 600 – 1400 °C in Ar and 10%H$_2$-Ar for 2 h	(highest BET surface at 900 °C)	- Faster reaction of coated W particles due to constant contact of reactants, H$_2$ also increases reaction rate - Full reduction in 10%H$_2$-Ar at 900 – 1000 °C, pure WC at 1100 °C - Direct WC formation without intermediate W2C (explanation by diffusion of C in W)	[23]
APT, TBO (W$_{20}$O$_{58}$)	CH$_4$	Milling of initial powder, parameters not specified	Reduction+Carburization: 850 °C and 820 °C for 2 h in 95%H$_2$-5%CH$_4$	<1 μm	- Reduction mechanism via solid state reaction (not CVT) due to dry atmosphere → small mean crystallite size - High carburization reactivity due to porosity creation during reduction step → good contact between W and CH4	[24]

2 Objectives of this Work

This work is a part of a comprehensive study focused on the effect of different carbon sources and processing atmospheres on the efficiency of reduction and/or carburization of WO_3 and W powders to obtain high purity fine grained WC powders. The two step synthesis process consists of mechanical activation of the precursors followed by a thermal activation in a reducing atmosphere.

Specifically the capability of optimized synthesis conditions based on published works in terms of achievable degree of carburization and WC grain size were investigated. Two different carbon sources (graphite and carbon black) were evaluated with respect to reactivity with W and WO_3.

Furthermore, based on the results, a deeper understanding of the individual contributions of carbon sources and CO atmosphere to reduction and/or carburization of the tungsten source as well as interactions between the precursors with the atmosphere are desired.

3 Materials and Experimental Procedure

Figure 1 gives an overview of different powder mixes that were prepared and how they were treated mechanically and thermally. Several material characterization techniques were used to analyze the powders at different synthesis stages. W-C mixes with mole ratios of 1:1 were prepared using two different carbon sources – graphite (G) and carbon black (CB). Additionally, WO_3 powder with the same two carbon sources with mole ratios of WO_3:C=1:4 were prepared.

Mechanical activation by ball milling followed by thermal activation in inert Ar atmosphere was carried out in order to assess the influence of different carbon sources on reduction and carburization.

The use of inert atmosphere (Ar) ensures that reduction and carburization is solely done by the solid admixed carbon sources. Additionally, the atmosphere's contribution to both reduction and carburization during thermal activation was investigated. To do so, tungsten oxide powder (WO_3) and pure tungsten powder with an average particle size of 1 μm (**W1**) were thermally activated in flowing gas mix of Ar-10 vol.% CO. Without the admixed solid carbon, reduction and carburization is carried out only by the CO containing atmosphere. Additionally, the effect of combined solid carbon and CO-containing atmosphere is evaluated.
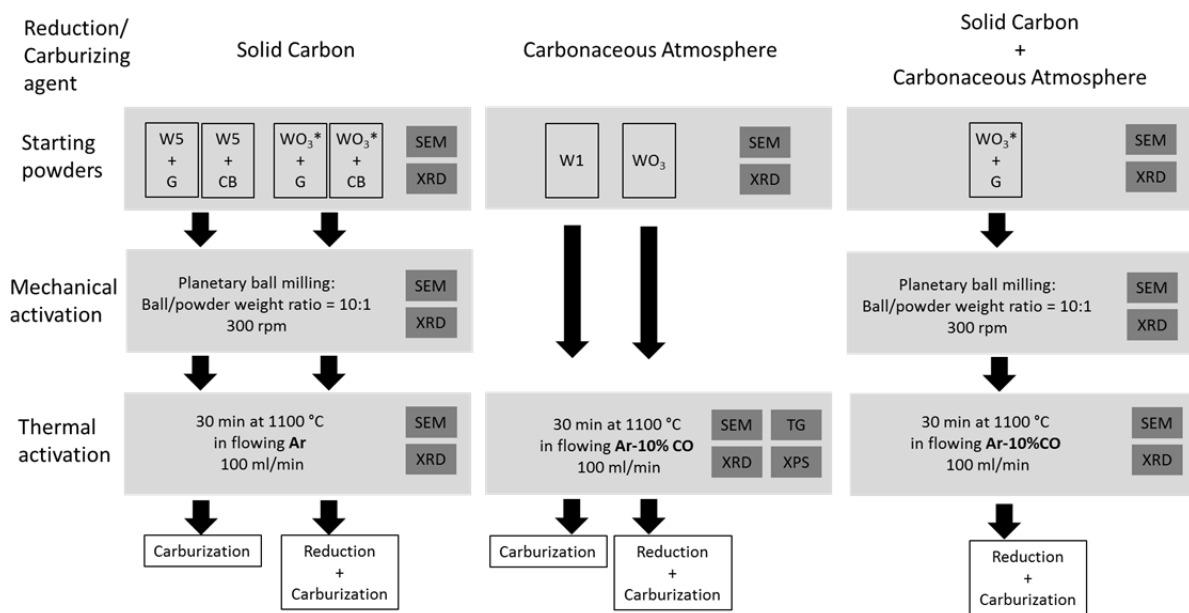

Figure 1: Overview of the experimental procedure. W5: W powder with 5 μm average particle size, W1: W powder with 1 μm average particle size, G: Graphite, CB: Carbon black, WO_3: Tungsten oxide

In the following chapters synthesis steps as well as characterization techniques will be described in more detail.

3.1 Starting Materials

The used tungsten and tungsten oxide powders were provided by Wolfram Bergbau- und Huetten AG (St. Martin, Austria). The two different carbon sources were provided by Imerys Graphite & Carbon (formerly TIMCAL Graphite & Carbon) (Bodio, Switzerland).

Characteristics of the base powder sources, according to manufacturers' data, are summarized in Table 3.

Table 3: Material specifications of the starting powders.

		W powder		WO_3 powder	Graphite Grade KS150	Carbon black Grade E250G
		"W1"	"W5"	WO_3	"G"	"CB"
BET	m_2/g			4.52	13	67
PSD FSSS	μm	0.87	4.4			
O content	ppm	3000	130			
Ash content	%				0.019	0.01
Fe content	ppm	<5	<5		32	6.3
Al content	ppm	<2	<2	<2	1	
S content	ppm	<5	<5		11	80
Ca content	ppm	<2	<2	<2	17	1.3
V content	ppm				19	<0.5
Mo content	ppm	17	<10	<10	0	
Si content	ppm	<10	<10	<10		59

Figure 2 shows SEM micrographs of the starting materials. As-received W5 powder consists of spherical particles of about 5 μm diameter. The used tungsten oxide powder consist of comparably coarse cubical particles in the range of about 20 up to 100 μm. Graphite shows the characteristic flake like morphology with flakes of several micrometers in size. Carbon black, on the other hand, exhibits an complex morphology with very fine nano-sized carbon particles forming big agglomerates (only agglomerates are visible on the micrograph).
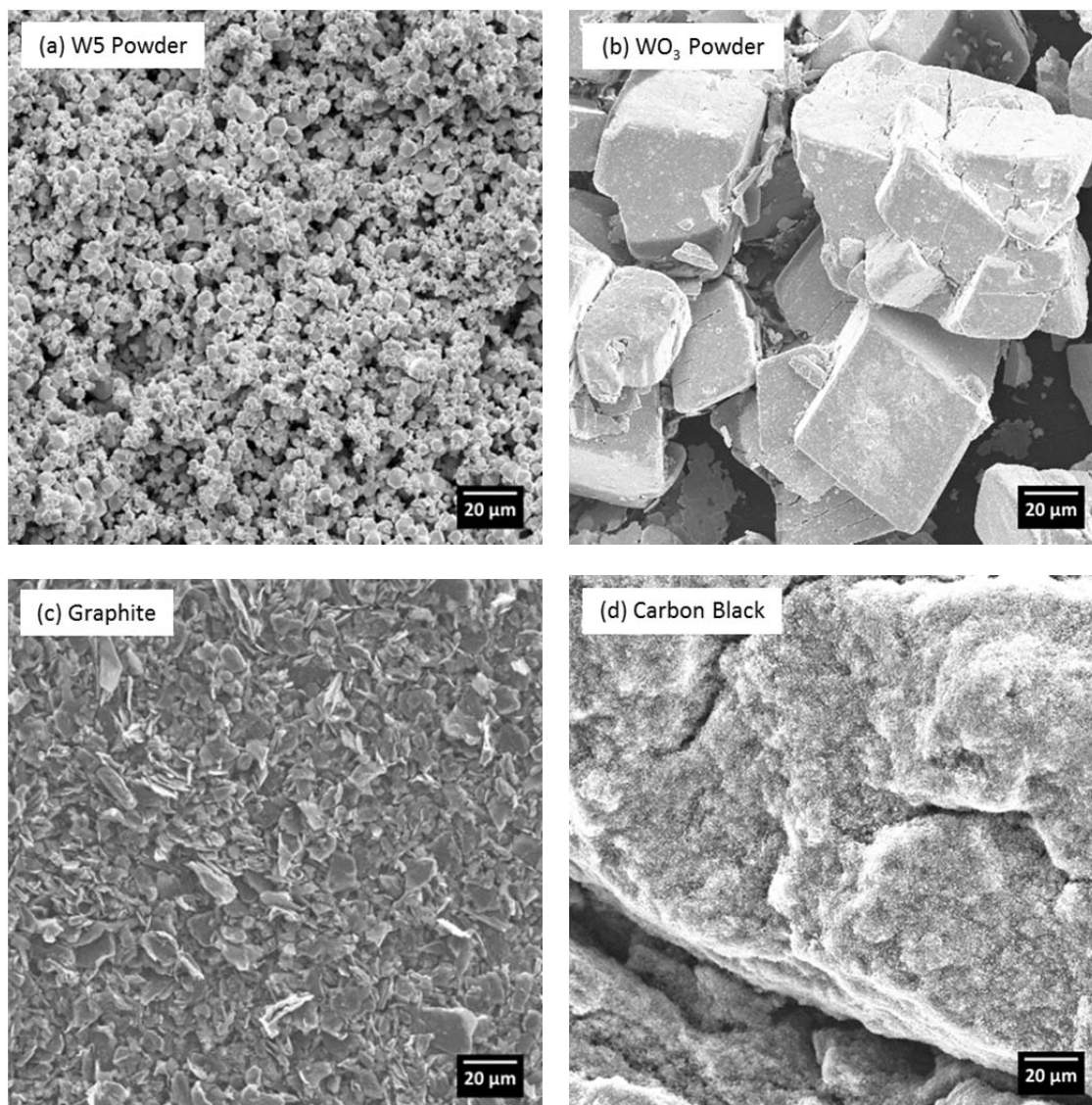
Figure 2: SEM micrographs of the as received starting powders used in the present study.

3.2   Planetary Ball Milling

Precursor mixes were subjected to mechanical activation in a planetary ball mill "Pulverisette 5" (Fritsch GmbH, Germany). The used bowl and balls (10 mm diameter) were both made of tungsten carbide. The ball to powder weight ratio was 10:1. Milling was performed at a rotational speed of 300 rpm for 2 hours for every mix. In order to minimize the temperature input, milling was interrupted every 15 minutes for 5 minutes as well as for 1 hour after 1 hour of accumulated milling time. Figure 3 shows an overview of the milling sequence.

Figure 3: Schematic of the ball milling sequence. Interruptions of milling were done in order to reduce the input of thermal energy. Pre-milling, solely of the WO_3 precursor powders was performed at the same conditions and following the same sequence as the precursor mixes.

3.3 Scanning Electron Microscopy

Mixes of the precursors after mechanical activation were analyzed regarding mixes` homogeneity and particle sizes. This was done by means of digital scanning electron microscope "DSM 940" by Carl Zeiss AG.

3.4 X-Ray Diffraction

The Scherrer equation (1) allows estimation of crystallite sizes in case of powdered samples [25][26]. It is based on the fact that the peak width (B) of a diffraction signal is inversely proportional to the average crystallite size normal to the corresponding diffraction plane (L).

$$B(2\theta) = \frac{K\lambda}{Lcos(\theta)} \tag{1}$$

Where θ is the Bragg angle where the reflection peak occurs, λ is the used X-Ray's wavelength and K is the Scherrer constant. The value for K is dependent on the method of the peak width determination (FWHM or integral breath) as well as the shape of the analyzed crystals [27].

In practice one has to carefully distinguish between different contributions to broadening of diffraction peaks. Apart from crystallite size, instrumental broadening depending on the experimental setup and used XRD equipment as well as micro-strains which displace the lattice of the analyzed material can give rise to broader diffraction peaks.

In the present study Bruker D8 Advance X-Ray diffraction instrument with CrKα radiation source (λ=2.2897 Å) was used. Matching of the diffraction patterns was based on the PDF-4 database provided by International Center of Diffraction Database (ICDD) [28]. Determination of the crystallite grain size by Scherrer equation was carried out from the three most intense peaks in the XRD patterns.

3.5 Thermogravimetry

Thermogravimetry (TG) is a thermal analysis method which allows to gain information on material properties such as thermal stability, sample composition, reduction and oxidation processes, etc. The mass of the sample is monitored while subjecting to a controlled temperature profile. Processing gases makes it possible to investigate interactions of the sample with the surrounding atmosphere. The instrumental setup of TG basically consists of chamber equipped with a highly sensitive microbalance containing the sample surrounded by a furnace following a desired temperature program. A constant

gas flow through the chamber can be achieved via inlet and outlet valves. Temperature measurement is done by an accurate thermocouple [29].

In this study an instrument designated as STA 449 F1 Jupiter by NETZSCH-Gerätebau GmbH [30] with a SiC furnace was used to investigate the interaction of different reducing and carburizing atmospheres with tungsten and tungsten oxide powders. An inert alumina crucible was charged with about 1 g of the respective loose powder (pure W or WO_3). The thermal treatment consisted of heating up the sample from room temperature at a rate of 10 °C/min to 1100 °C followed by an isothermal holding time of 30 min. Powder samples were subsequently cooled down to 50 °C at a programmed cooling rate of 30 °C/min. The investigated atmosphere was introduced by a constant gas flow of Ar and/or Ar-10 % CO mix at a flow rate of 100 ml/min lasting from the beginning of the heating cycle until the sample was at about 225 °C during the cooling step. Except for the change of atmosphere, all other parameters were kept constant throughout this study.

3.6 X-ray Photoelectron Spectroscopy

X-ray Photoelectron Spectroscopy (XPS) also known as Electron Spectroscopy for Chemical Analysis (ESCA) is a surface sensitive material characterization technique. Qualitative analysis (meaning identification of elements or chemical states) as well as quantitative analysis of only a few atomic layers beneath surfaces is possible.

The basic principle lies in the photoelectric effect which causes atoms being irradiated by x-rays to emit electrons. These electrons are having a certain kinetic energy (E_k) according to:

$$E_k = h\upsilon - E_b - \phi_s$$

(2)

Where hν is the exciting X-ray photon's energy, E_b is the binding energy of the emitted electron and φ_s is the work function of the spectrometer. The transition of the emitted electron undergoes is illustrated in Figure 4 [31].
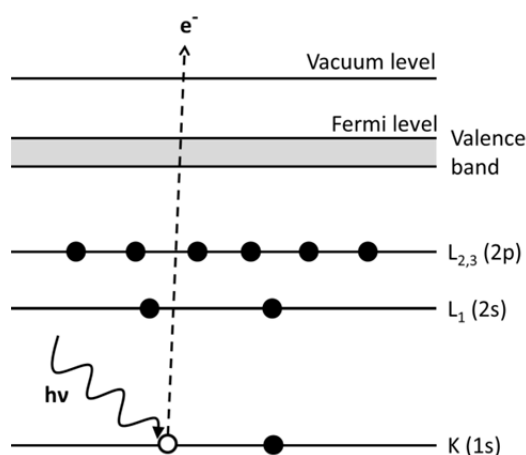

Figure 4: Schematic of a photoelectron emission process. An electron in the K shell is excited by an incoming X-ray photon with energy hν and subsequently leaves the system while creating a vacancy. Redrawn from [32].

A photon excites an electron in an inner orbital which causes the electron to leave the atom leaving behind a hole in the electronic configuration. Every element has a unique electronic configuration which in turn results in photoelectrons with very specific kinetic energies according to the photon's interaction with electrons from different orbitals. Therefore it is possible to identify all elements

except for hydrogen. However, according to equation (2) the emitted electron's energy depends also on the exciting photon's energy hν. Therefore, it is important to irradiate the sample with monochromatic X-rays [31] in order to obtain less artifacts in the measured spectra.

After the photoelectron emission, a consecutive relaxation process takes place. An electron from an outer orbital fills the previously generated hole. Due to the energy difference of the two orbitals a specific excess energy is generated. This energy can either be emitted in the form of an X-ray photon or be transferred to another electron. The excited electron which eventually leaves the atom is referred to as an Auger electron. Figure 5 schematically shows the process of relaxation described [32].
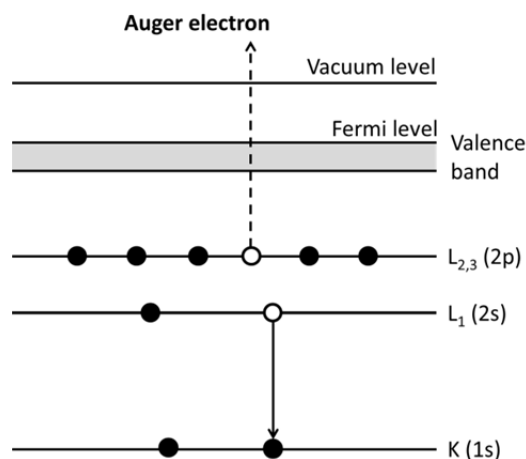

Figure 5: Auger electron emission. The previously created vacancy is filled by an electron from an outer shell. Its excess energy is transferred to another electron that subsequently leaves the atom. Redrawn from [32].

The above seen Auger process is a $KL_1L_{2,3}$ process. The XYZ type notation is standard in this context where X stands for the core hole (here K) that is filled by an electron from Y level (here L_1). The final Auger electron then leaves from level Z (here $L_{2,3}$). The Auger electron's energy (E_A) is:

$$E_A = E_K - E_{L_1} - E_{L_{2,3}} - \phi_S \tag{3}$$

E_K, E_{L1} and $E_{L2,3}$ are the energies of the corresponding electron levels according to Figure 4 and φ_S is the work function of the spectrometer. The Auger electron emission occurs about 10^{-14} seconds after the initial photoelectron process. Auger electrons are another way of qualitative analysis. Their specific energy is independent of the exciting photon's energy [32].

Electrons originated from both processes undergo inelastic scattering with atoms and molecules while they are travelling to the detector. This phenomenon is responsible for the high surface sensitivity of only a few nanometers since only electrons emitted from there have sufficient kinetic energy to escape from the interior and eventually reach the detector [32].

Depending on whether the atoms emitting the photoelectrons are in elemental state or forming compounds with other atoms, the local electron configuration is slightly changed. The specific kinetic energy of the generated photoelectrons will therefore be slightly changed as well. This is reflected in the shift of the individual spectral lines in the spectra. Since these shifts depend on the type of bond, oxidation state and the electron configuration of the corresponding bonding partner atoms, it is possible to identify the chemical state of the elements present as well as formed compounds [33].

A broad survey scan is usually done initially in order to roughly evaluate the chemical composition. It is then followed by more detailed scans in narrow energy ranges of interest. Different types of lines

can be used for chemical analysis. The most distinct peaks are photoelectron peaks but also Auger lines can be seen. Spectra also show phenomena such as X-ray satellites, X-ray ghosts and shake-up lines [31].

Experimental Setup

The used instrument in this study is PHI 5500 (PERKIN ELMER, Eden Prairie, Minnesota, USA) which is equipped with a monochromatic Al K_α X-ray source with characteristic emission at 1486.6 eV. During analysis the chamber was at condition of ultra-high vacuum (10^{-9} mbar). The angle between both X-ray source and spectrometer to the normal of the sample holder was 45°. The position of the ion gun was at 50.5° from the sample surface. Powder samples were prepared by pressing loose powder into Al plates. The circular area being analyzed while measuring was about 0.8 mm in diameter.

For the purpose of depth profiling ion etching with Ar^+ ions was carried out with ionizing voltage of 4 kV. The etching rate was calibrated using flat oxidized tantalum foils with known thickness [34]. Subsequent analysis and peak fitting in order to deconvolute the recorded spectra were performed with PHI Multipak software.

4 Results and Discussion

Characteristics of the mixes of W powders and carbon sources are presented first since they largely determine the reactivity of the mix during following thermal activation. Secondly results of thermal activation of these precursor mixes and pure tungsten sources in inert or carbonaceous atmosphere are presented. Results are divided depending on whether solely carburization or both reduction and carburization are carried out by the corresponding carbon sources.

4.1 Mechanical Activation

The purpose of the mechanical activation is to mill and evenly distribute the precursors to ensure large contact areas. Only then effective reaction between them can take place. Four mechanically activated powder mixes (two of W with carbon sources and two of WO_3 with carbon sources) are qualitatively characterized considering the degree of homogeneity of the mix and comminution of the WO_3 particles.

4.1.1 Mixes of Tungsten with Different Carbon Sources

Characteristics of the mixes of W powder with graphite and carbon black after ball milling are presented in SEM images in Figure 6. Mixing and milling of W powder with both carbon sources according to the stated conditions provides effective particle size reduction of the prcursors to sub micron size. After milling the flaky structure of graphite is no longer recognizable (at the used magnification) which indicates breaking down of the graphite particles. Moreover the mixes are homogeneous but contain bigger agglomerates which are shown in more detail in Figure 7. Different carbon sources don't seem to have an influence on the effectiveness of milling since the mixes show same morphological features.
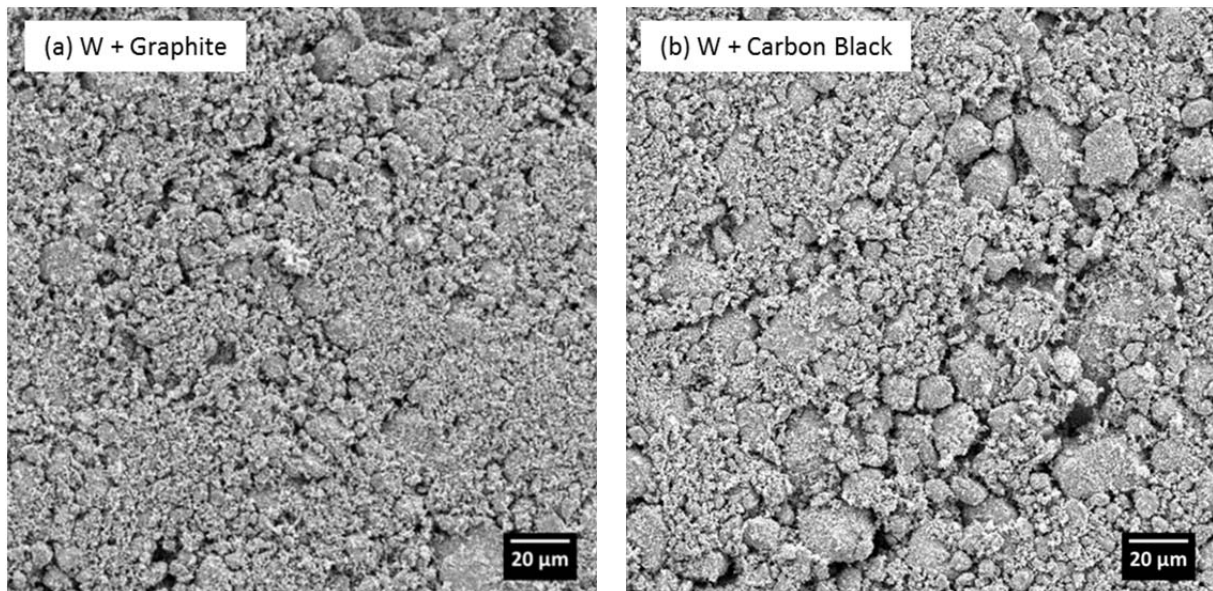

Figure 6: SEM micrographs showing the efficiency of two hours ball milling in terms of particle size reduction and homogeneity of the mix in case of W powder with the two investigated carbon sources (Graphite and carbon black).
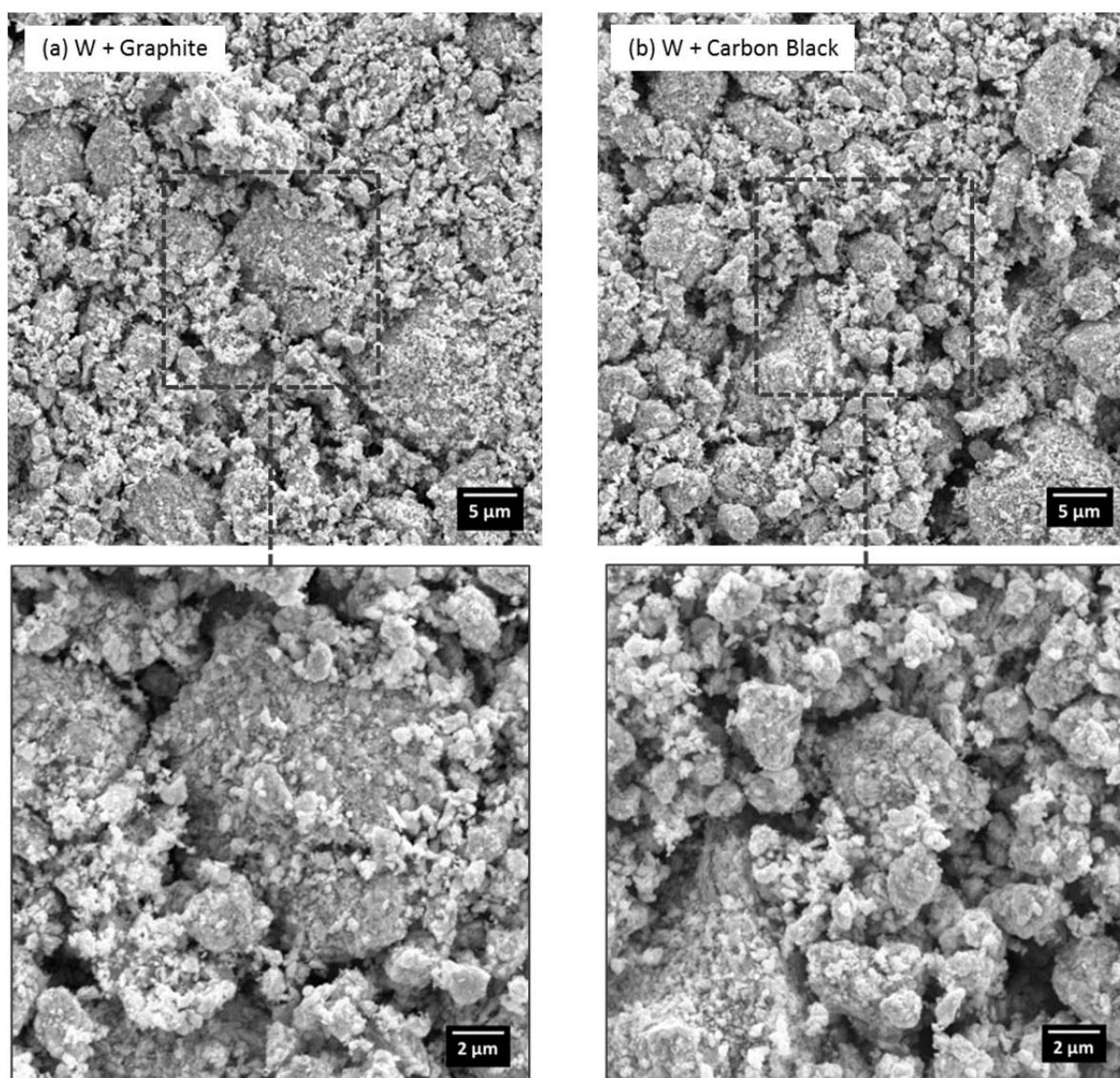
Figure 7: SEM micrographs of the W-carbon mixes at higher magnifications after ball milling showing individual particles and their agglomerates.

Measured XRD patterns of the as-received W powder and mixes with the carbon sources followed by ball milling are shown in Figure 8. Apart from characteristic tungsten peaks (designated as W) the as received tungsten powder (5µm particle size) shows a low intensity peak at 41.3° (designated as X) which, according to the available database, matches either chromium tungsten oxide (Cr_2WO_6) or rutile which is a polymorph of titanium oxide (TiO_2). Analysis by EDX as well as XPS however did not show presence of Cr or Ti. It is also possible that a tungsten oxide phase with the same structure as rutile is present. In any case, the formed phase originates from the tungsten source and is not a result of the milling procedure. The phase's peak intensity however seems to increase during milling.

After milling both mixes with graphite and carbon black show peak broadening in the XRD pattern which can be attributed to the tungsten crystallite size reduction and build-up of internal strains in the crystal lattice. In both cases no new phases are formed after ball milling and the patterns look identical for graphite and carbon black. The absence of a graphite peak shows that the energy introduced by the milling procedure is sufficient to break down the ordered graphite structure. There are no differences observable between mixes containing graphite and carbon black which is in agreement with the conclusion made from the SEM analysis.
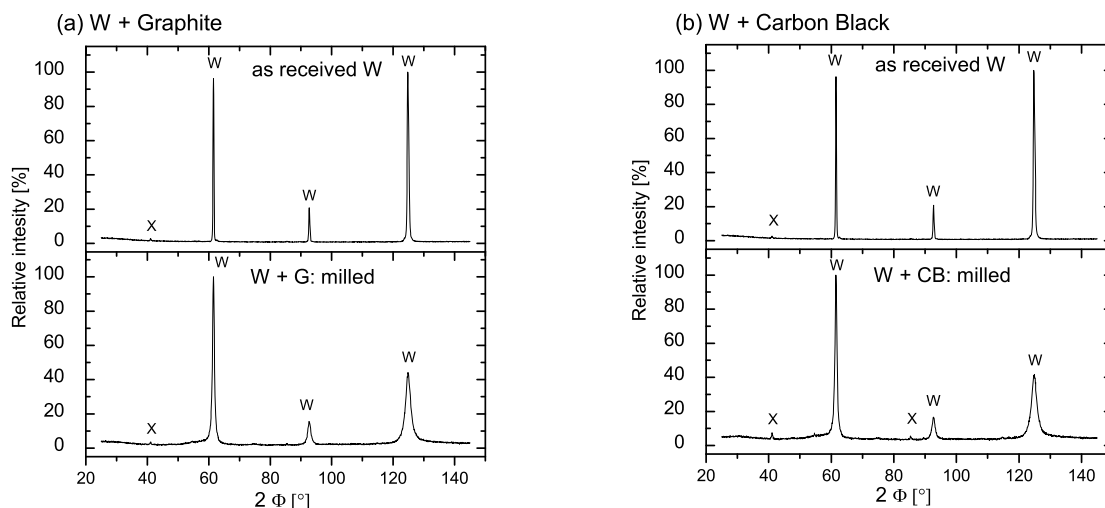
Figure 8: XRD patterns of the two W-carbon mixes as compared to the as received W powder (5 µm particle size).

4.1.2 Mixes of Tungsten Oxide with different Carbon sources

Figure 9 shows SEM images of the WO_3 containing mixes. As previously described there are issues of hampered comminution during milling arising from increasing carbon content [35]. In order to counteract the negative effect of higher carbon amount on the milling efficiency, the as received tungsten oxide (about 20 to 100 µm particle size, see Figure 2) was milled separately for 2 hours before admixing to the carbon (see Figure 10). Then the mix containing carbon and pre-milled WO_3 was milled for another 2 hours. The tungsten oxide-carbon mixes obtained after this process appear comparably fine and homogeneous as the corresponding tungsten-carbon mixes. A severe reduction of the initial tungsten oxide particle size has therefore taken place.
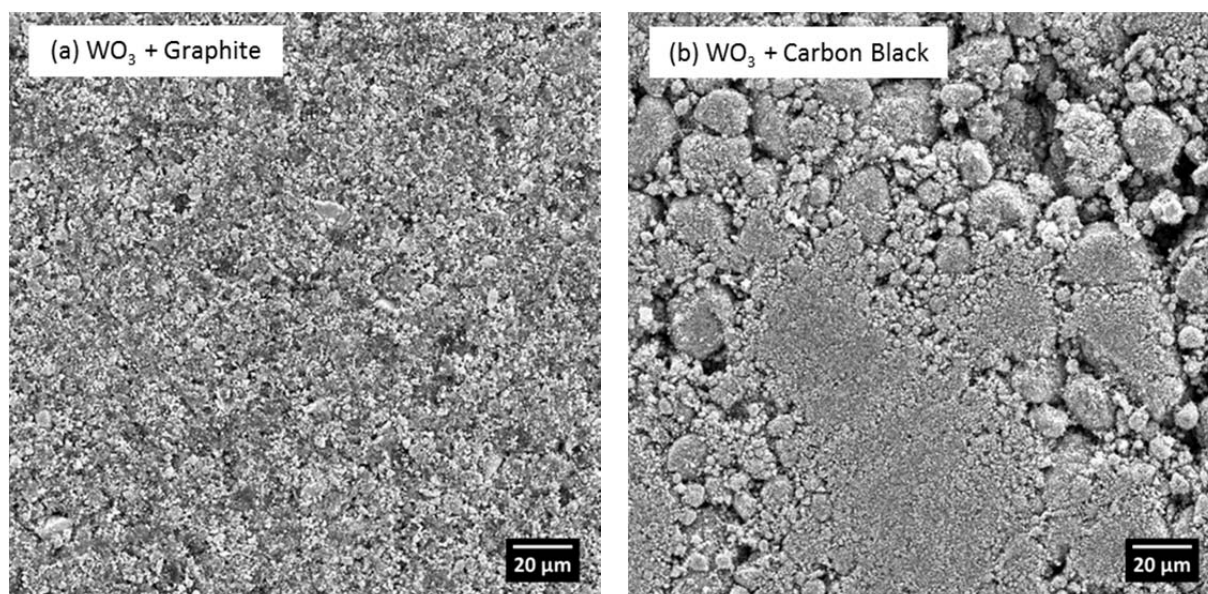

Figure 9: SEM micrographs showing the efficiency of ball milling and the resulting homogeneity of the WO_3-carbon mixes. As received WO_3 powder was pre-milled separately for 2 h followed by 2 h milling together with the admixed carbon source.
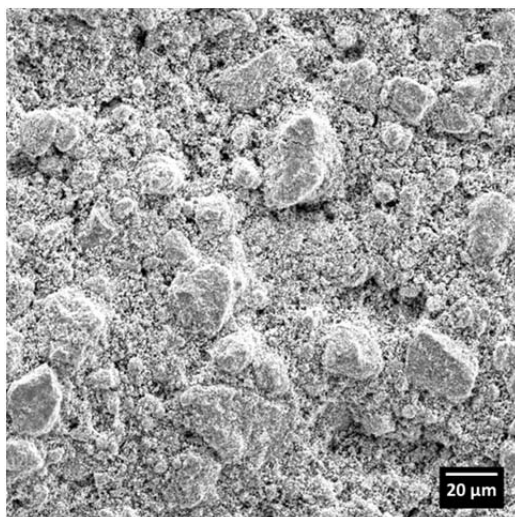
18

Figure 10: SEM micrograph of the WO$_3$ powder after pre-milling.

SEM images at higher magnification in Figure 11 show the mixes' particle morphologies after the two ball milling steps in more detail. Particle sizes appear slightly bigger (up to 2 µm diameter) in the graphite containing mix as compared to the mix with carbon black. Furthermore, presence of graphite flakes after milling can be observed which is different from the W-containing mix in Figure 7 where no graphite was distinguishable after milling. The higher magnified SEM micrographs therefore indicate slightly less effective milling conditions for WO$_3$-carbon mixes, especially in case of graphite.

As compared to the previously shown W-carbon mixes there is a higher amount of admixed carbon present (WO$_3$:C mole ratio = 1:4) which is necessary for initial reduction of tungsten oxide to metallic W followed by carburization. This causes difficulties with obtaining fine and homogeneous WO$_3$-carbon mixes arising from the soft character of carbon black and graphite. In this study these problems were counteracted by pre-milling of WO$_3$ separately, and the mixes obtained present better properties than those reported in previous studies where no pre-milling was carried out [35]. The obtained mix quality, however, is still slightly worse as compared to tungsten-carbon mixes, especially in graphite containing mix, probably due to the lubricating effect caused by graphite. The lubricating effect of graphite is attributed to sliding of its individual layers of hexagonally bound carbon atoms since they are held together by comparably weak van-der-Waals forces.
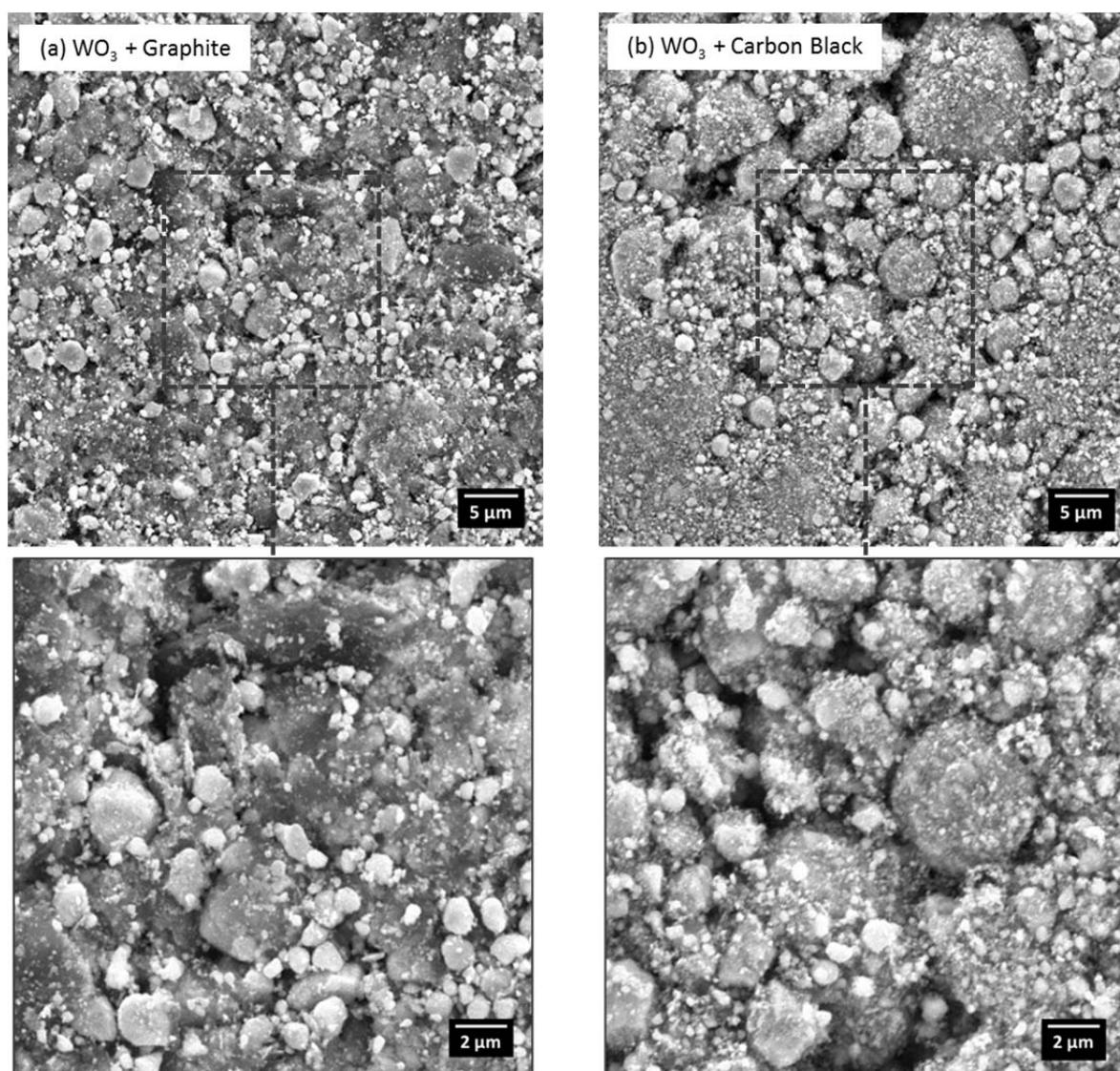
Figure 11: SEM micrographs of the WO$_3$ mixes at higher magnification with graphite and carbon black after ball milling showing individual particles and their agglomerates.

Figure 12 summarizes the measured XRD patterns of tungsten oxide powder in the as received state and for the mixes with carbon after milling. No newly formed phases are observable indicating that there are no phase transformations induced by the provided mechanical energy. Broader reflection peaks after ball milling indicates reduction of tungsten oxide crystallite size and/or generation of internal lattice strains during milling of both mixes. This effect seems to be less pronounced in case of graphite and can be attributed to its lubricating effect and so less effective milling. In contrast to the tungsten-carbon mixes, graphite is still present after ball milling as seen in the spectrum. However, comparison of the as-received graphite (see Figure 13) with the mix in Figure 11 (a) shows a significant reduction of the graphite particle size (initially around 20 μm) after milling. After ball milling together with the tungsten oxide particles, graphite flakes are still distinguishable besides tungsten oxide particles but are of smaller size.
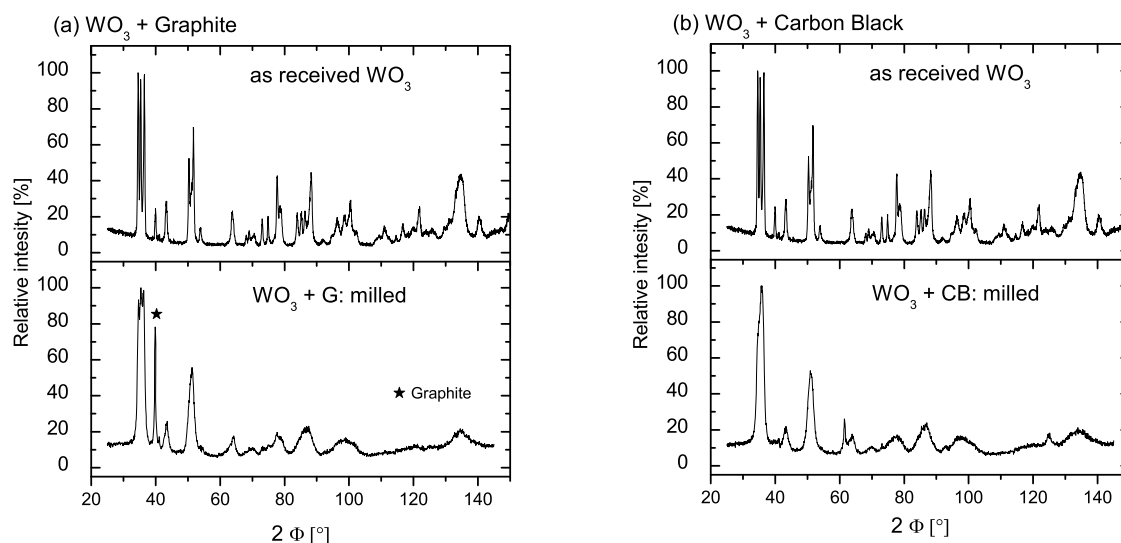
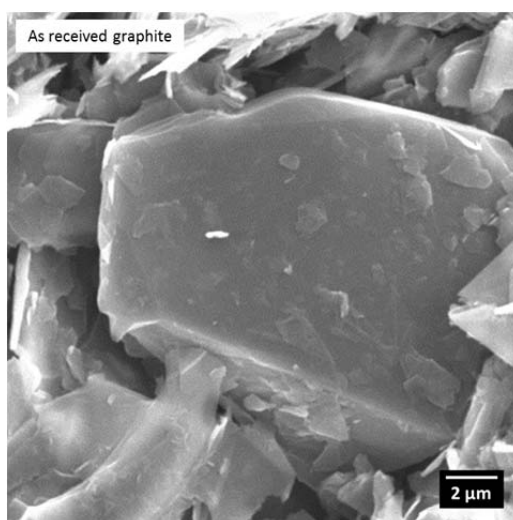Figure 12: XRD patterns of the two WO_3-carbon mixes as compared to the as-received WO_3 powder.

Figure 13: SEM micrographs showing as-received graphite.

4.2 Thermal Activation

During thermal activation the mixed precursors are subjected to a heat treatment to provide the required temperature for the diffusion controlled reactions of reduction and/or carburization. Presence of reactive atmosphere can assist those processes. The previously prepared W and WO_3 mixes with the corresponding carbon sources are thermally activated and the formed phases are analyzed. Except for the atmosphere, conditions of thermal activation are kept constant during the different synthesis experiments.

4.2.1 Carburization of Tungsten Powders

The prerequisite for complete carburization is the constant supply of carbon to the surface of the reacting particle. Three cases are looked at within this study where carbon is provided by:

21

(1) Solid carbon
(2) Gaseous CO
(3) Solid carbon and gaseous CO

Solid carbon which is in direct contact with W particles is believed to react directly and provide efficient carburization. However carbon particles which are not in direct contact still contribute to the carburization, the exact reaction mechanisms and interactions of the reaction partners during carburization are still not completely understood.

One suggested mechanisms occurring during carburization of W particles is summarized in the following paragraph [23][10]:

Figure 14 shows a sketch of the proposed mechanism. The initial step of carburization is a surface reaction of W and the carbon source to form an activated carbon atom C* on the W-particle surface which subsequently diffuses into the bulk W. Initially the high carbon availability at the W particle surface lets a WC shell grow. Further carburization is limited by the diffusion of C* through the WC shell. Diffusion of carbon in WC is slower as compared to W_2C and W. The mechanisms are vacancy diffusion where carbon atoms move between interstitial sites of the metal lattice. The limited C* supply for the interior W core particle results in formation of an inner shell of W_2C which starts growing inwards in radial direction. Eventually the whole interior consists of W_2C while the outer fully carburized WC shell still stays at about the same thickness. Further C diffusion through the WC shell finally causes full carburization of the particle interior.
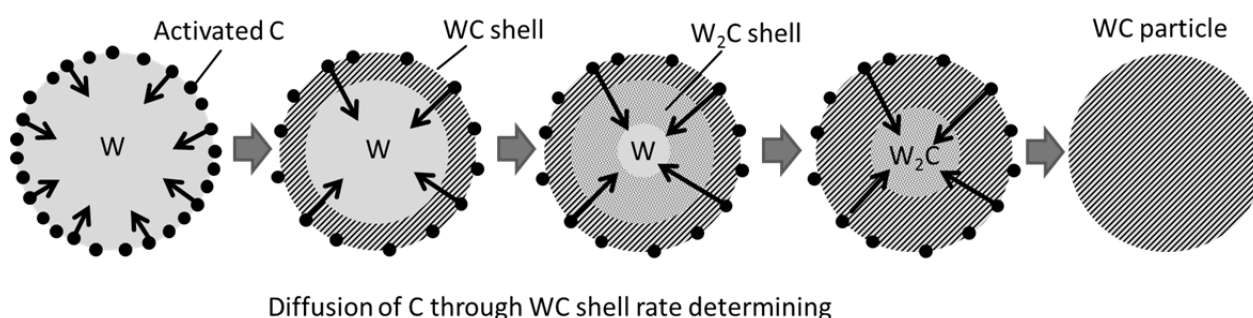

Figure 14: Sketch of reaction mechanism occurring during carburization.

A. Carburization by Solid Carbon

Figure 15 shows the XRD patterns after thermal activation of the W-carbon mixes in Ar atmosphere. Apart from minor peaks corresponding to the previously described phase X, WC is the only phase detected which suggests full carburization by both graphite and carbon black. Both patterns seem identical which gives no indication of different carburization efficiencies of the two carbon sources. The mixing and carburizing conditions at 1100 °C for 30 min in pure Ar atmosphere are therefore sufficient for WC synthesis from pure tungsten powder. The relative intensity of phase X, however, increases during the thermal activation process. In case of graphite this effect is more pronounced as compared to the synthesis from the carbon black containing mix.
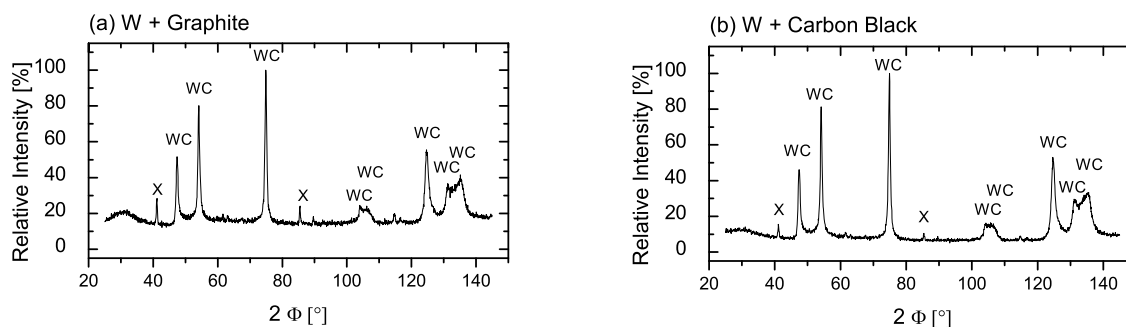
Figure 15: XRD patterns after thermal activation of the W-graphite and W-carbon black mixes for 30 min at 1100 °C in Ar atmosphere.

The morphology of the two fully carburized powders is shown in Figure 16. Individual particles are to a large extent in sub-micron range and are forming bigger agglomerates in both samples. No significant changes in morphology or particle size as compared to the particle characteristics before thermal activation (Figure 11) were observed.
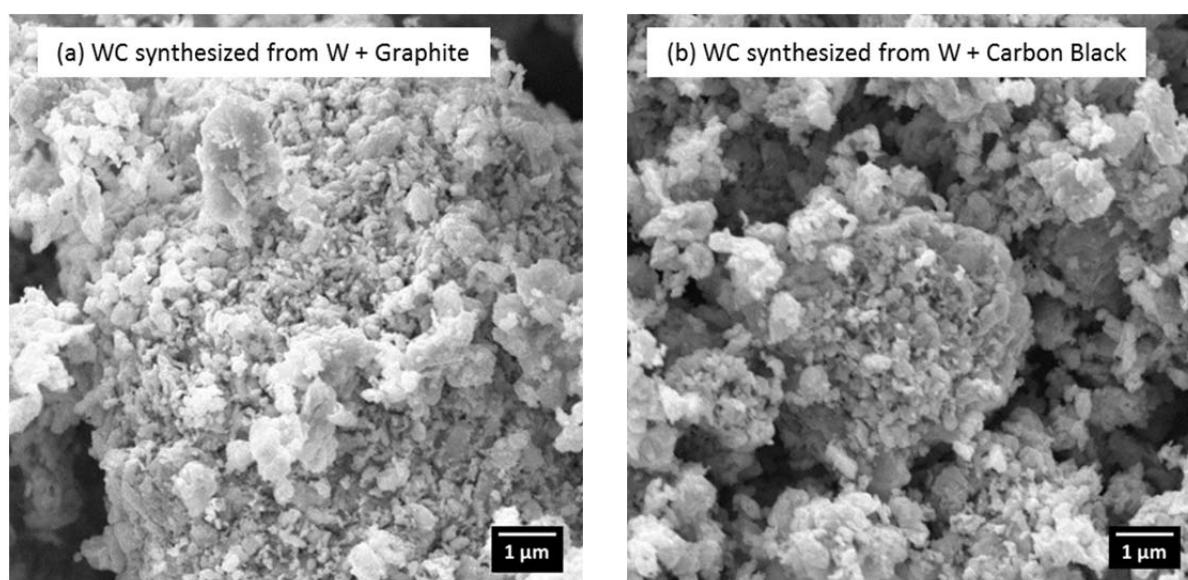

Figure 16: SEM micrographs of WC particles after synthesis by mechanical and thermal activation of (a) W-graphite and (b) W-carbon black mixes.

Estimated crystallite sizes at the different stages of synthesis are shown in Figure 17. The as received tungsten powder (5 μm particle size) consists of crystallites of about 44 nm size. Subsequent ball milling with graphite and carbon black yields in reduced WC crystallite sizes of 59 % and 61 %, respectively. After transformation to WC during thermal activation at 1100 °C for 30 min in Ar the estimated grain size is about 23±3 nm in both cases which is an increase of about 24 % from the W crystallites after mechanical activation. Error bars show the standard deviation from the average crystallite size estimated from the three most intense reflection peaks. Individual WC particles, as seen in Figure 16, consist therefore of several crystallites
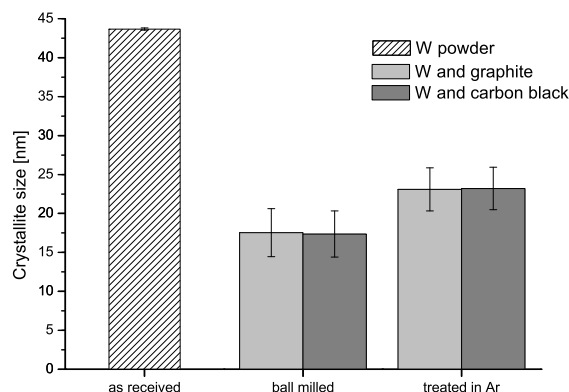
Figure 17: Estimated crystallite sizes throughout synthesis of tungsten carbide from tungsten-carbon mixes synthesized in pure Ar atmosphere. Estimation was done according to Scherrer equation [26] applied to the three most intense reflection peaks of W (as received, ball milled) and WC (after treated in Ar) in the corresponding XRD patterns (see Figure 8).

Complete carburization of tungsten-carbon mixes (W:C mole ratio = 1:1) after mechanical and thermal activation for both carbon sources suggests that the applied milling procedure provides beneficial starting conditions for the synthesis of nanocrystalline WC. This can be attributed to the high contact area between the precursors, which was confirmed by SEM and XRD analysis, and highly-deformed structure of the base tungsten powder, providing more effective diffusion of carbon into the powder core. Subsequently, carbon diffusion into W which is the rate determining process in case of the solid-solid reaction, is enhanced. The type of carbon source doesn't show differences in carburizing efficiency for the investigated synthesis parameters.

B. Carburization by CO-containing atmosphere

Thermogravimetric analysis carried out in case of W powder in Ar-10%CO atmosphere is shown in Figure 18. Regarding mass change there is loss of 0.40 % until the end of the isothermal holding at 1100°C for 30 min followed by a mass gain of 0.11 % until the end of the process. Hence, the overall mass loss is 0.3 %. Therefore, three different processes can be distinguished:

(1) 0.12 % loss in the temperature range 30-500 °C (0-47 min) can be attributed to decomposition of adsorbed species on the powder particles.

(2) In the temperature range 825-850 °C the reduction of oxide layer on the W powder particles starts. There is 0.24 % mass loss until the end of the isothermal.

(3) 0.11 % gain starting immediately at the end of isothermal holding at 1100 °C. Possible reactions occurring are either oxidation or carburization by the atmosphere. XPS investigation performed on Ar-10%CO treated W powder will give some conclusions in the following chapter.

Furthermore an inflection in the mass loss graph at about 970 °C (or DTG peak) suggests the start of another process or change in reaction kinetics. It can be speculated that this is the actual onset of carburization which happens after majority of surface oxide layer was reduced, however, reduction is still ongoing. Carburization from the CO means carbon uptake from the atmosphere which is accompanied by mass gain. Subsequently the overall mass loss is counteracted and the corresponding slope becomes less steep.
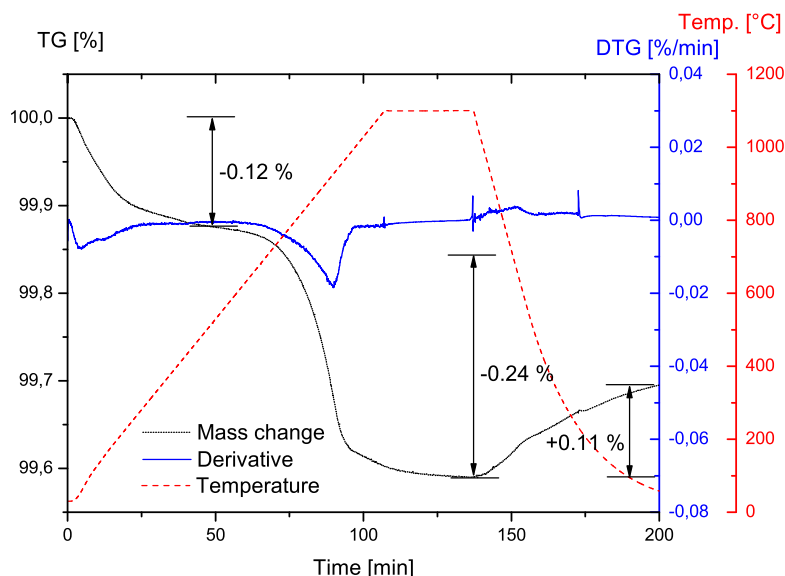
24

Figure 18: Thermogravimetry graph of tungsten powder during heat treatment in Ar-10%CO atmosphere. Heating rate is 30 °C/min, isothermal holding time 30 min at 1100 °C followed by cooling at an average rate of ~30 °C/min to 300 °C.

Results of chemical analysis (provided by Höganäs AB) with regard to carbon and oxygen content of the W powder before and after the heat treatment in Ar-10%CO are summarized in Table 4. A carbon uptake of about 0.023 wt.-% and oxygen loss of 0.294 wt.-% were measured. The theoretical overall mass loss according to chemical analysis is therefore 0.271 wt.-% which is in agreement with 0.3 wt.-% mass loss from TG analysis. The majority of the mass change is therefore due to the reduction of surface oxide layers on the powders. The small carbon uptake suggests carburization.

Table 4: Results of chemical analysis on the W powders before and after thermal activation in Ar-10%CO atmosphere.

	C content [wt.-%]	O content [wt.-%]
As received	0.007	0.3
After treatment in Ar-10% CO	0.03	0.006
	$\Delta m=+0.023\%$	$\Delta m=-0.294\%$

XRD measurements in Figure 19 (a) show no presence of WC phase after heat treatment in Ar-10%CO. There is however a slight increase in W crystallite size to 39±2 nm from initially 36±2 nm in the as received state (see Figure 19 (b)).
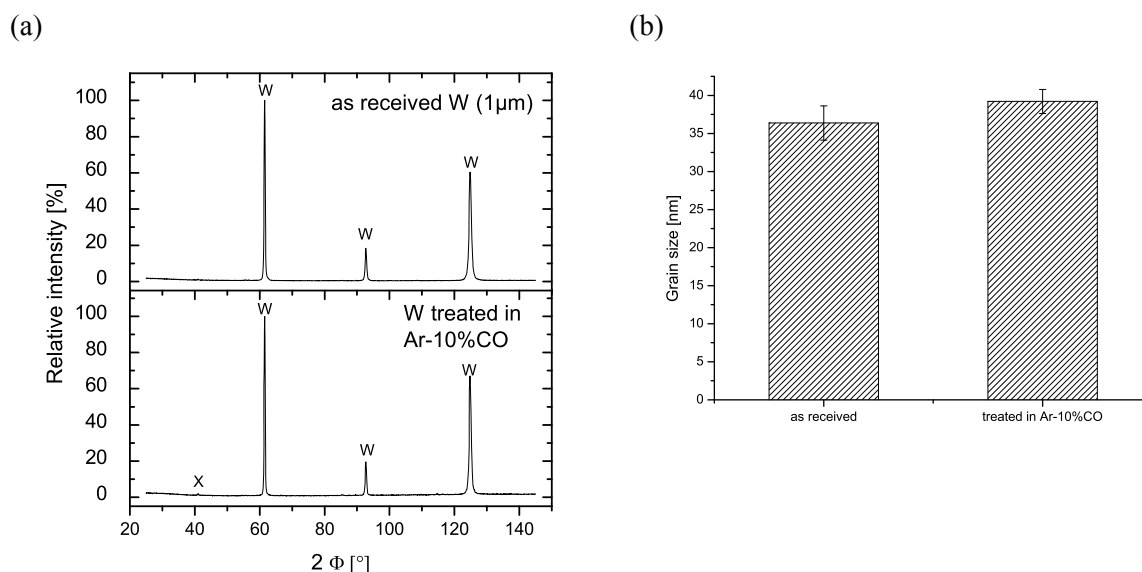
25

(a)   (b)

Figure 19: (a) XRD patterns of as received tungsten powder and after treatment in Ar-10%CO atmosphere at 1100°C for 30 min. (b) Estimated tungsten crystallite size for both powders according to Scherrer equation [26] applied to the three peaks in the XRD pattern.

Even though no formation of W_2C or WC could be detected by XRD analysis, mass gain which was observable from TG analysis along with the gain of carbon revealed by chemical analysis suggests some degree of carburization. The formed phases are probably below the detection limit of XRD and located preferably on the powder surface according to the model presented in Fig. 13. Hence, surface analysis techniques capable of detecting lower concentrations like XPS are required to detect presence of carbide layer on the powder surface.

The XPS spectrum of tungsten powder treated in Ar-10%CO gas for 30 min at 1100 °C was compared to spectra of as received tungsten and tungsten carbide powders. The spectra of tungsten and tungsten carbide are used as references for the initial, untreated tungsten powder and the desired fully carburized powder. Changes from the initial tungsten spectrum towards the tungsten carbide spectrum occurring during the CO treatment can be indications for carburization.

Initial broad survey scans of all the three samples showed minor traces of impurities. Figure 20 shows the spectrum of as received W powder as an example. Specifically carbon originating from adsorbed carbonaceous species and small traces of sodium. In all cases the corresponding signals were only detectable on the surface and disappeared after a few nm of ion etching. Oxygen peaks present in the spectra indicate the presence of an oxide layer formed on top of the particles.
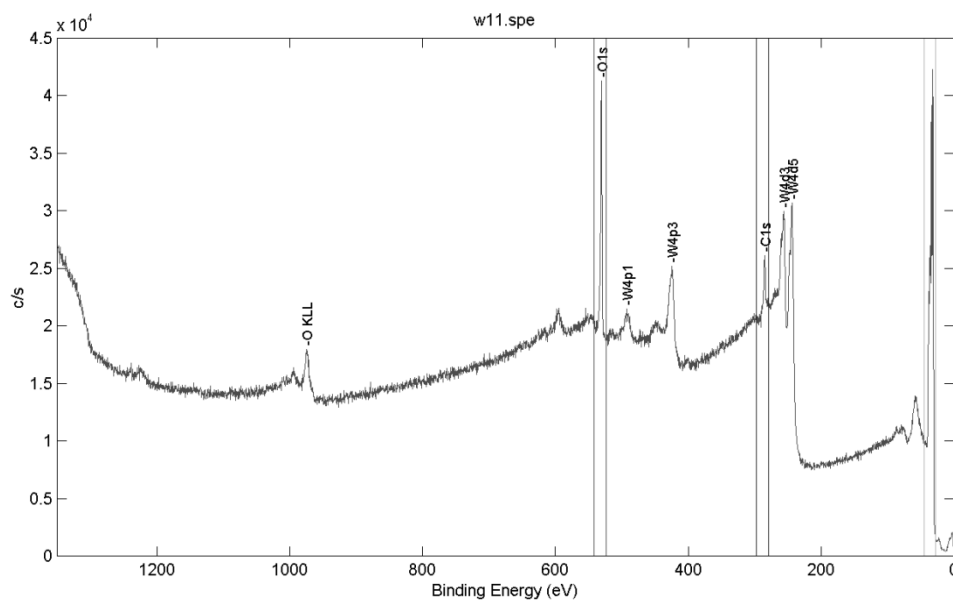
Figure 20: XPS survey scan of as received W powder.

Detailed narrow scans were performed in three energy regions in order to identify chemical shifts and compounds based on the following spectral lines:

- 29-42 eV around W5p3, W4f5 and W4f7 lines
- 280-292 eV around C1s line
- 527-538 eV around O1s line

Figure 21 gives an overview of all detailed scans performed on the analyzed powders at 4 different etching depths.
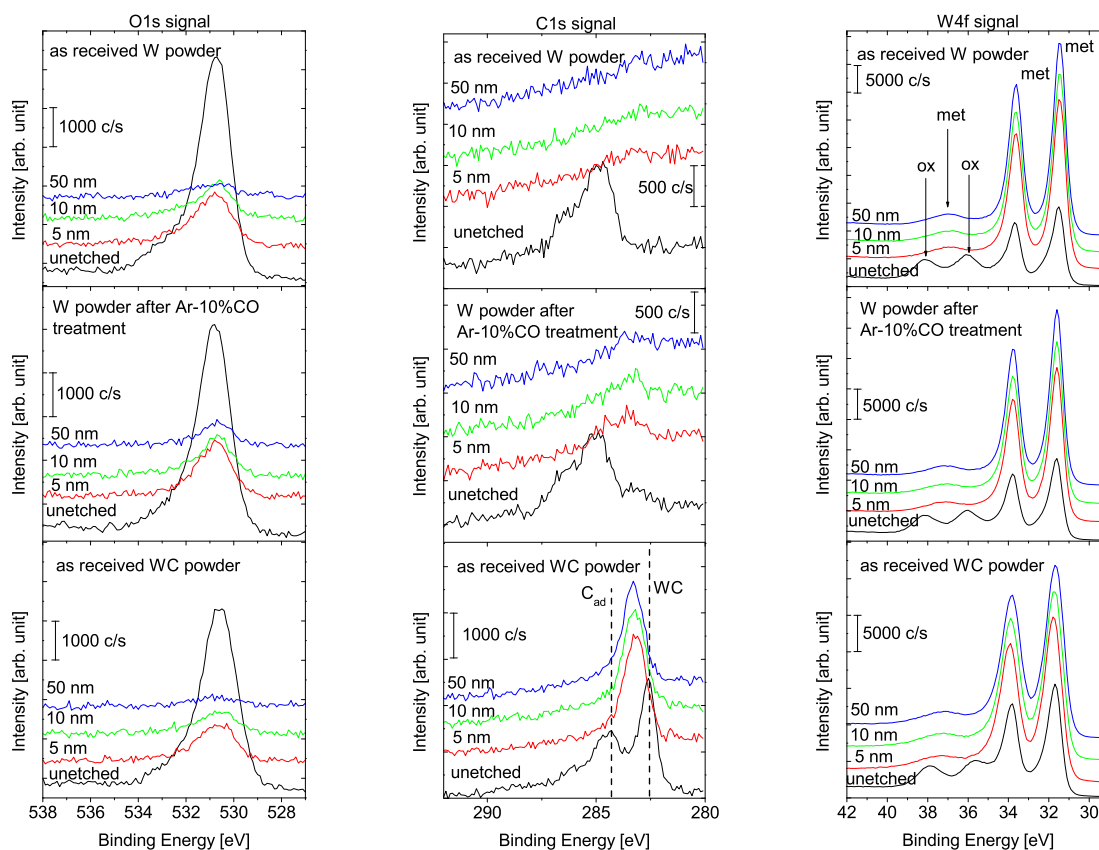
Figure 21: Detailed XPS scans of the as received W powder, after thermal activation in Ar-10%CO and of as received WC powder at different etchings.

The recorded photoelectron peaks positions are summarized in Table 5. Presence of WO_3 in the spectra of as-received state (see also Figure 21) suggests that all three analyzed powders are covered by a tungsten oxide layer of type WO_3.

Table 5: Overview of the relevant peak positions corresponding to the analyzed elements in their chemical states.

Element	Chemical Formula	Spectral line	Peak positions [eV]		
			W powder as-received	W-treated in CO	WC powder as-received
W	W	W5p3	37.0	37.1	-
	W	W4f5	33.6	33.8	-
	W	W4f7	31.5	31.6	-
	WO_3	W4f5	38.1	38.2	37.9
	WO_3	W4f7	36.1	36.0	35.7
	WC	W5p3	-	-	37.3
	WC	W5f5	-	-	33.9
	WC	W5f7	-	-	31.8
O	WO_3	O1s	530.7	530.8	530.7
C	C	C1s	284.8	284.9	284.3
	WC	C1s	-	-	282.6

Figure 22 shows the chemical composition plotted as a function of etch depth for the three analyzed powders. The elemental concentration was estimated by calculating the ratios of the areas under the C1s, O1s and W4f peak while taking the sensitivity factors of 0.314, 0.733 and 3.863 respectively into

account. Rather high contents of oxygen and carbon of ~43 at.-% and ~21 at.-%, respectively, in the unetched state of as received W powder originate from oxidation and contamination by adsorbed carbonaceous species on the particles' surfaces. After 3 nm ion etching the carbon concentration is reduced towards trace amount which stays constant throughout further etching. Oxygen concentration is reduced to a stable value of ~10 at.-% after about 15 nm etching.

As-received WC powder in unetched state shows slightly elevated carbon concentration of ~45 at.-% followed by leveling off at ~35 at.-% after about 5 nm ion etching which removes adsorbed carbon-containing species. The initial oxygen concentration of ~28 at.-% is lower as compared to W powder and also reduces significantly to a stable value of ~2 at.-% after about 15 nm of ion etching. Those comparably lower oxygen concentrations indicate lower oxidation of the powder surface and thinner oxide layers formed on WC particles.

W powder which was processed for 30 min at 1100 °C in Ar-10%CO exhibits the same tendency of elevated oxygen and carbon concentration of ~35 at.-% and ~38 at.-% in the un-etched state followed by leveling off at ~10 at.-% after about 10 nm ion etching for both oxygen and carbon. The carbon concentration is higher than in case of untreated as received W powder at any etching depth investigated which is an indication of carburization.
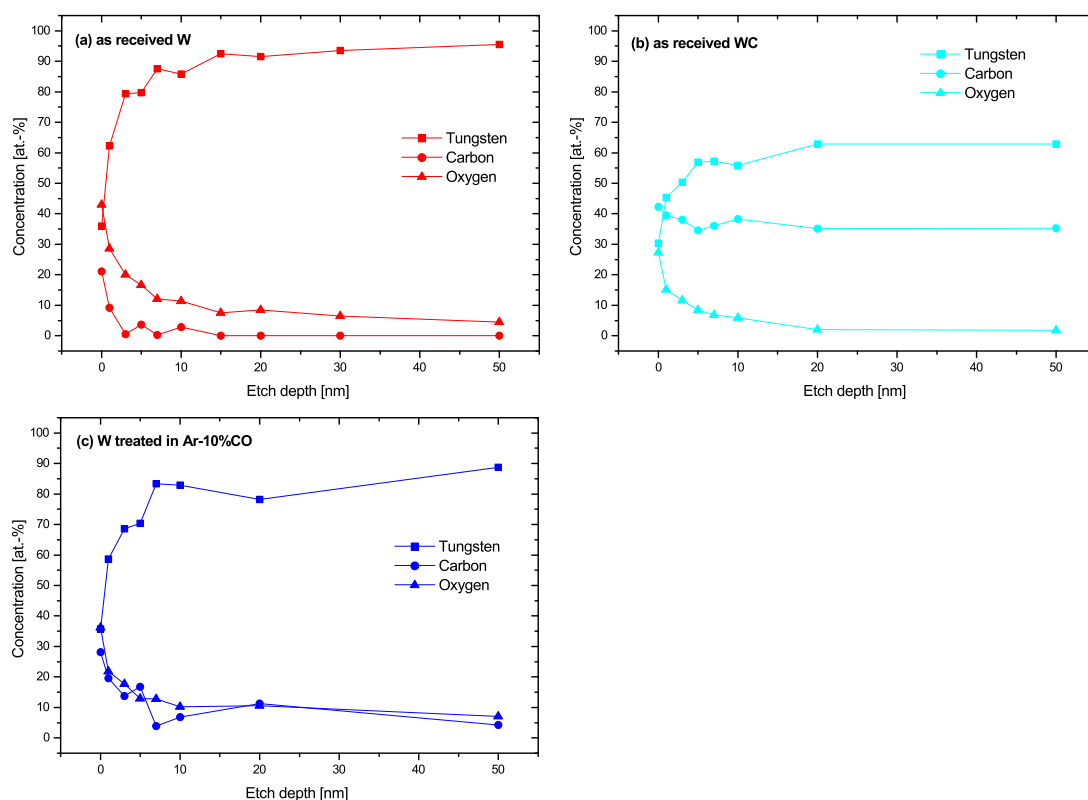

Figure 22: Chemical composition as function of etch depth for (a) as received tungsten powder, (b) as received tungsten carbide powder and (c) tungsten powder treated in CO atmosphere for 30 min at 1100 °C.

Normalized carbon concentration is shown in Figure 23. All three analyzed powders show an initial reduction of carbon concentration due to removal of adsorbed carbonaceous species while ion etching. It can be seen that W powder treated in Ar-10%CO shows a lower gradient of carbon concentration as compared to the untreated, as received state.
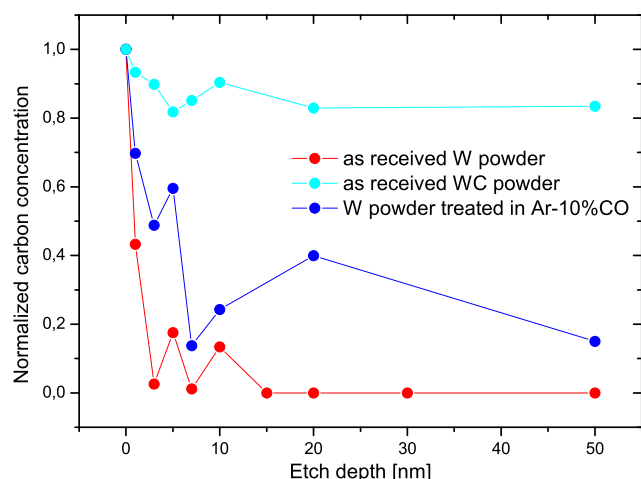
Figure 23: Normalized carbon concentration as a function of etch depth for as received tungsten powder, powder after treatment in Ar-10%CO and of as-received WC powders.

Analysis of fraction of tungsten in different chemical states (metallic, bound in WC and oxidic) was done by curve fitting in the energy range of the W5p3, W4f5 and W4f7 peaks (for positions see Table 5). Previously mentioned oxide layers covering the powder particles have an influence on the carburization process since they constitute a diffusion barrier for carbon and hence need to be reduced first.

There are ways of estimating the oxide layer thicknesses on powder particles by combining XPS with ion etching technique as described in literature [34][36]. Those studies are based on a model which takes all the difficulties that may arise when analyzing irregular shaped surfaces into account. In contrast to a flat surface, a sample for analysis consists of a large number of powder particles. This results in irregularity of the analyzed surface. Shading effects as well as angle dependent variation of the X-ray flux, photoelectron intensity and ion sputter rate are hence present. It was shown that it is possible to estimate the thickness of a homogeneous surface oxide on a spherical particle at a certain value of the relative intensity of the substrate [34]. The thinner the oxide layer gets during the etching procedure, the higher the fraction of analyzed substrate material gets.

Figure 24 shows the relative intensity of the W^{met} and W^{WC} signal as a function of etch depth for the three analyzed powders. The graph comprises curves of increasing metallic relative intensity value with etching depth due to the increasing metallic contribution after sputtering.
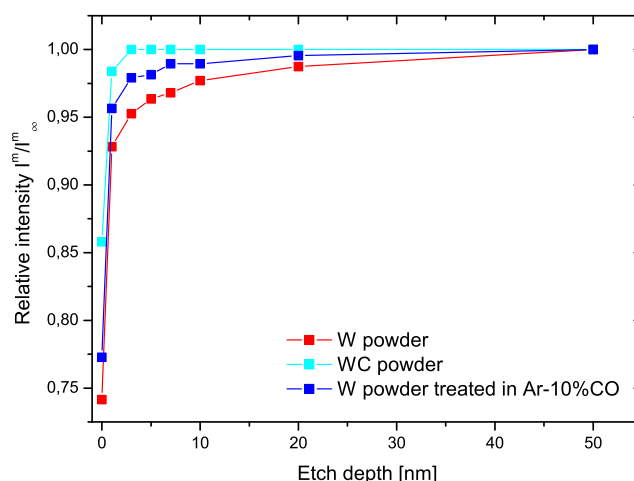
Figure 24: Relative metal intensities of the W4f7 signal peak as a function of etch depth of as received W and WC powder and of as received W powder after thermal activation in Ar-10%CO atmosphere at 1100 °C for 30 min.

The relative intensity of the metallic signal in the unetched state is 0.74, 0.77 and 0.85 for the cases of as received W powder, after thermal activation in Ar-10%CO and as received WC powder respectively. Since there is a significant fraction of metallic signal present in all cases, the oxide layer is assumed to be smaller than the electron attenuation length of W4f electrons in a WO_x matrix. Chemical state analysis of tungsten with XPS (see high resolution spectra in Figure 21) shows that the oxide covering the powder particles is WO_3. Attenuation length of W4f7 photoelectrons with E_{kin}=1451.3 eV through a WO_3 layer was calculated to be 28.07 Å and 28.03 Å for W4f5 photoelectrons (E_{kin}=1449.1 eV) [37]. Values for kinetic energy were calculated according to equation (2) in chapter 3.6 with a work function of 3.9 eV for the used equipment. The ratio of oxide thickness and electron mean free path is in the range of: $0 < t^{ox}/\lambda^{ox} \leq 3$. According to [34] the relative metal intensity at an etching depth corresponding to the oxide thickness needs to be in the range of $0.73 \leq I^m/I^m_\infty < 1.0$. Taking the mean value of that range i.e. $I^m/I^m_\infty \sim 0.86$, as a rough estimation, the oxide layer thickness of the three powders is given by the intercept of a horizontal line at 0.86 relative intensity with the corresponding curve. Accordingly the layers are < 1 nm thick. Insignificant differences between the powders at that relative intensity, however, make quantification not reasonable. Due to the decreasing relative metal intensity values, oxide thickness increase in the order WC – W powder treated with Ar-10%CO – W powder. Hence, this indicate lower oxide layer thickness after treated in Ar-10% CO, pointing to the reduction of oxide layer on as-received W powders by CO.

In order to evaluate the carburization process Figure 25 compares high resolution narrow scans around the C1s peak of the as received W and WC powders with W powder after treatment at 1100 °C for 30 min in Ar-10%CO atmosphere. As-received W and WC powders act as references of the initial state and the desired fully carburized state. In case the thermal treatment in Ar-10%CO atmosphere causes carburization the spectrum should change from the as-received W powder towards the as-received WC powder. Unetched states and after etching of 5, 10 and 50 nm are plotted. In the unetched state all three powders indicate presence of a peak at about 285 eV binding energy. Those originate from adsorbed species which contain carbon atoms and disapear after the first etching step.

The spectrum of WC additionally contains its C1s peak located at 282.6 eV binding energy at all etching stages. This WC specific peak is subjected to slight shifting throughout depth profiling caused by changing of WC stochiometry due to the selective ion etching.

After removal of the adsorbed carbon compounds, observed on as-received W powder, spectra at 5, 10 and 50 nm do not show any presence of carbon. After treatment in Ar-10%CO atmosphere at 1100 °C for 30 min, the powder's spectrum in the unetched state shows signs of a small low intensity peak in the same binding energy range as the carbide signal in case of the WC powder. This peak was observed during further etchings while decreasing in intensity. Even at 50 nm ion etching the peak is still distinguishable. The absence of this peak in the as received W powder is a clear indication for some degree of carburization.

Apart from WC, W_2C is a possible intermediate phase formed during carburization. According to literature, there is a slight shift of the C1s signal from 283.5 eV to 284.1 eV [40][42] or from 283.1 eV to 283.6 eV [43] when comparing WC to W_2C. The weak, noisy nature of the C1s signal recorded in the spectra of the W powder treated in Ar-10%CO, however, makes establishment of the exact binding energy in the presented study impossible. Subsequently, formation of W_2C as a intermediate product of carburization cannot be verified. The lack of extensive XPS data on W_2C makes a final conclusion very inaccurate.
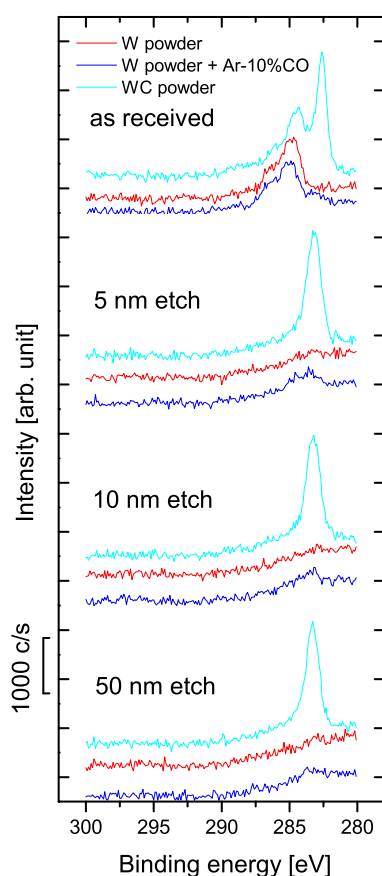

Figure 25: Evolution of the C1s signal in XPS spectra of as received tungsten powder, powder after treatment in Ar-10%CO and tungsten carbide powders at different etching depths.

4.2.2   Reduction and Carburization of Tungsten Oxide Powders

According to an extensive study by Venables et al. [44][45] carbothermal reduction of WO_3 occurs in two main stages: $WO_3 \rightarrow WO_2$ and $WO_2 \rightarrow W$. Depending on the characteristics of the precursors regarding particle size, mix preparation and impurity content different starting temperatures for the reduction process in the range of ~655 – 780 °C are reported [10]. The composition of the processing atmosphere also plays a role [10].

The suggested mechanism for the reduction by solid carbon is presented in Figure 26. Initially direct reduction by solid carbon which is in contact with the oxide particle reacts (see reaction (1) in Fig.26) and due to the formation of gaseous CO a porous outer layer of WO_2 (possibly also $WO_{2.72}$) is created. Since WO_3 and carbon are not in direct contact anymore, indirect reduction by CO via reactions (2a) and (2b) takes place. CO needs to diffuse from the exterior through the porous WO_2 structure to the interior non-porous WO_3 where reduction occurs. The reduction product CO_2 simultaneously diffuses outward. Throughout the whole reduction process, supply of CO is ensured via reaction (3). Diffusion through the outer porous shell is the rate determining and reacting particles consist of a shrinking dense core of unreduced WO_3 surrounded by a growing shell of porous, partly reduced WO_2. Eventually the whole particles are reduced to WO_2 and the second stage begins. Now further indirect reduction takes place via reaction (2b). The rate limiting step is now reaction (3).This is due to fast diffusion and easy access of CO and CO_2 to the corresponding reaction sites and the higher CO content required for reduction from WO_2 as compared to WO_3 which can be seen in Figure 27. After reduction is completed the resulting W particles are smaller as compared to the initial WO_3 particle size.

In case of WO_3 reduction in absence of solid carbon but in reducing CO atmosphere, the discussed mechanism changes in the sense that reduction is indirect and only via reactions (2a) and (2b) [46]. Initial direct reduction and interaction between the solid carbon source with the processing atmosphere are absent.
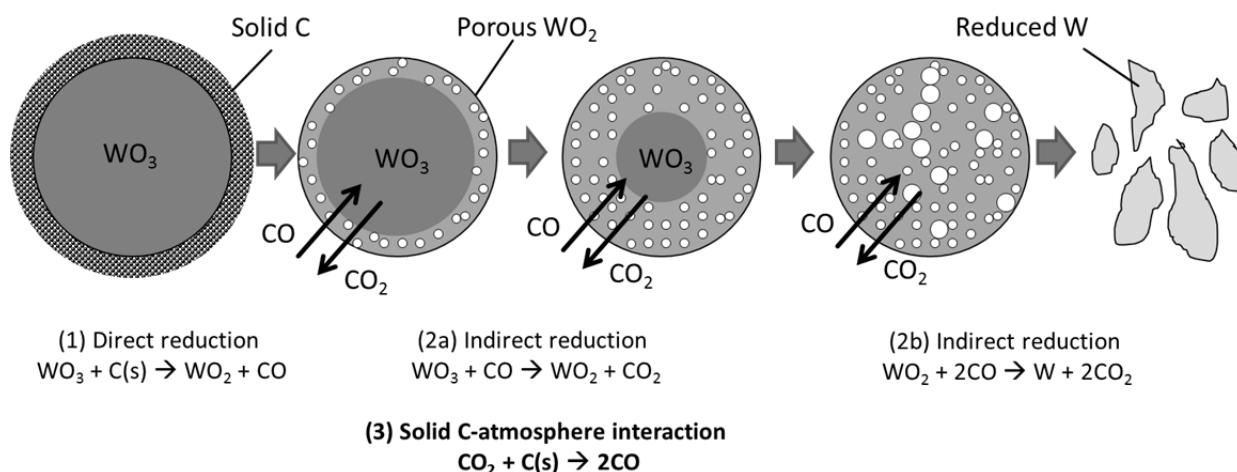

Figure 26: Sketch of reaction mechanism during reduction of WO_3 by solid carbon. Both direct and indirect reduction occur.
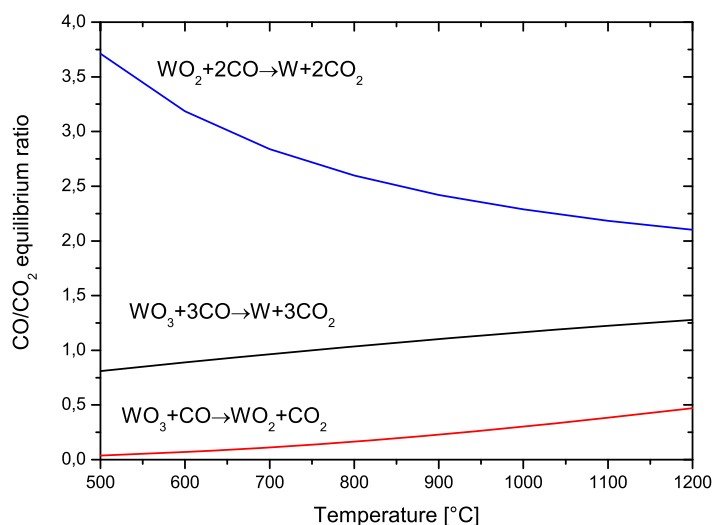
Figure 27: The equilibrium ratios of CO/CO2 for the relevant reduction steps. Data obtained by thermochemical simulation software "HSC Chemistry" Version 7.1.

According to a study performed by Koc et al. the carburization process starts as soon as activated C* atoms can form on the metallic W particle surfaces (see chapter 4.2.1). In this context it was observed that if formation of C* is very fast due to quick reduction and/or good availability of carbon at the W metal surface direct WC formation without previous transformation to W_2C can occur. Diffusion of C in W is the limiting reaction step in this case [23].

A. Reduction and Carburization by Solid Carbon

After thermal activation of WO_3-carbon powder mixes, the change in the phase composition is determined by XRD. The recorded patterns are shown in Figure 28. Absence of tungsten oxide reflection peaks after thermal activation at 1100 °C for 30 min in pure Ar for both mixes indicates complete reduction. Mass losses of 30.04 % for graphite and 28.92 % for carbon black containing mixes are close to the theoretical mass reduction of 30.02 % accompanied by reduction via $WO_3 + 3C \rightarrow W + 3CO(g)$ followed by carburization via $W + C \rightarrow WC$. Differences in the reduction efficiency of the two investigated carbon sources cannot be seen.

The following carburization process is not completed after 30 min at 1100 °C in both mixes since W and W_2C are present. The conditions of thermal activation are therefore not sufficient in terms of temperature and/or isothermal holding time for complete carburization. The carbon black containing mix however shows a significantly higher WC/W_2C ratio and therefore higher carburization efficiency is provided by carbon black. Results of quantitative analysis of the XRD patterns are shown in Table 6. A possible cause is the slight less efficient mechanical activation observed in SEM analysis in case of graphite. The lower WO_3-carbon contact area, also connected to significantly finer size of carbon black particles in comparison with graphite, subsequently decreases diffusion efficiency of carbon and reduction followed by carburization is therefore slower. There is, however, a smaller portion of pure un-carburized W in the graphite containing mix. This suggests that graphite somehow benefits the initial carburization of W particles towards the intermediate phase W_2C while further carburization to WC is promoted by carbon black.
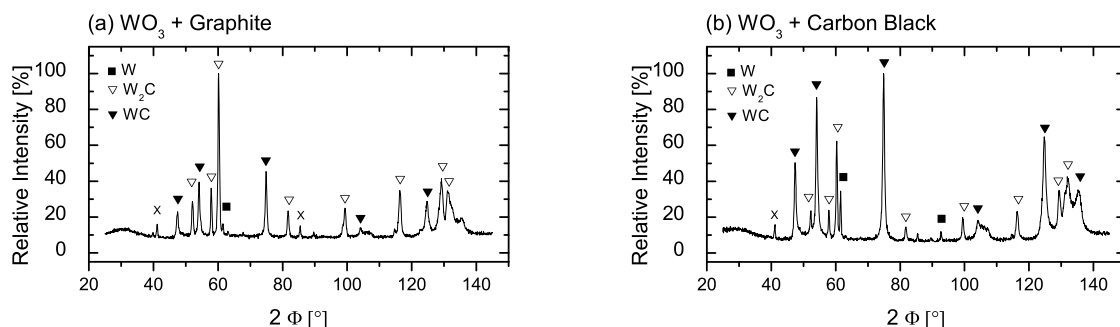
Figure 28: XRD patterns recorded after thermal activation of the WO_3 powder-carbon mixes in Ar

Table 6: Phase composition after thermal activation of WO_3-carbon mixes, obtained by XRD analysis.

Phase	Content [%]	
	WO_3 + Graphite mix	WO_3 + Carbon black mix
W	2 %	12 %
W_2C	79 %	43 %
WC	19 %	45 %

Figure 29 shows SEM micrographs of the two mixes of WO_3 with carbon sources after thermal activation in Ar. As compared to the initial morphology of the mixes before thermal activation (see Figure 11) the particle sizes seem to be homogenous and in sub-micron range. The porous character of the agglomerates is a result of disintegration of oxide particles during reduction which is accompanied by formation of gaseous CO. Similar particle morphologies were reported elsewhere [47][48]. Furthermore, no remaining graphite flakes are observable which is in agreement with the XRD results.
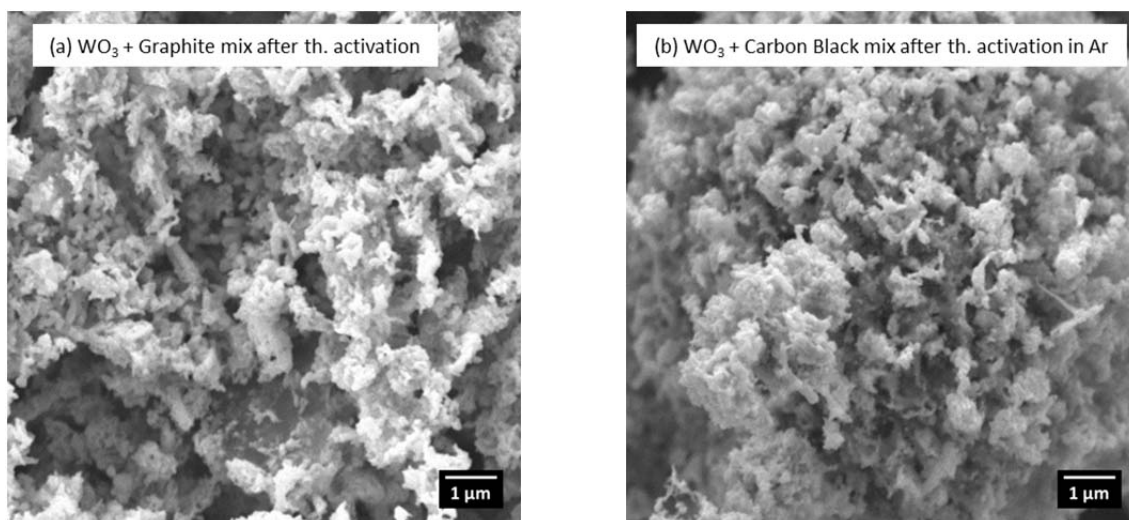

Figure 29: SEM micrographs of the WO_3-carbon mixes after thermal activation in Ar. Particles consist of W, W_2C and WC.

Due to the complexity and overlap of many reflection peaks in the XRD pattern of WO_3, crystallite size estimation by Scherrer equation was neither performed in the as received nor the ball milled state. Sizes of the WC crystallites synthesized from graphite and carbon black are however 26±4 nm and 25±2 nm, respectively. Direct WC synthesis with present mixing, milling and thermal activation parameters therefore results in nano-crystalline WC. The type of carbon source seems to have no

significant influence on the WC crystallite size. WO_3 and graphite, however, leads to slightly larger WC crystallite size as compared to both W-carbon mixes (chapter 4.2.1).
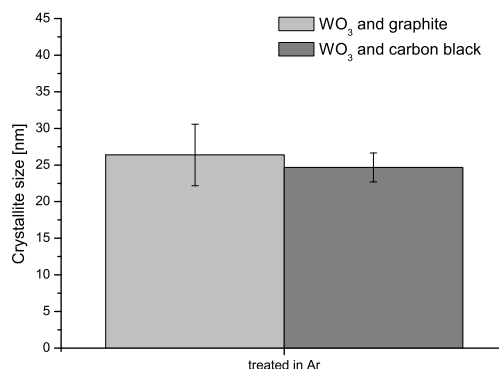

Figure 30: Estimated crystallite sizes of tungsten carbide phase formed after thermal treatment of tungsten oxide-carbon mixes in pure Ar atmosphere. Estimation was done according to Scherrer equation [26] applied to the three most intense WC reflection peaks in the corresponding XRD pattern (see Figure 12)

Similarly to W-carbon mixes, nano-crystalline WC of about the same crystallite size is formed from WO_3. However, to obtain pure WC similar to W-carbon mixes an increase of thermal activation temperature/time is necessary which in turn would cause grain growth and so result in larger grains.

The type of carbon source seems to have no significant influence on the WC crystallite size.

B. Reduction and Carburization by Gaseous CO

Thermogravimetric analysis carried out during thermal activation of WO_3 powder in Ar-10%CO atmosphere is shown in Figure 31. Total mass loss during heating stage and isothermal holding at 1100 °C is 2.40 % followed by a mass increase of 0.06 % during cooling stage. Some processes can be distinguished from the mass change graph:

(1) Mass loss of 0.12 % in the range of 30-500 °C due to evaporation of adsorbed species from the particle's surface.

(2) Main mass loss which can be attributed to the reduction of the WO_3 particles starting in the range of 850-900 °C. Until the end of the isothermal holding there is 2.28 % mass loss.

(3) Slight mass gain of 0.06 % during cooling stage most probably due to reoxidation starting at a temperature of 675°C .

An inflection in the mass-change graph after about 15 min at the isothermal heating at 1100 °C indicates a change in reduction type/kinetics.
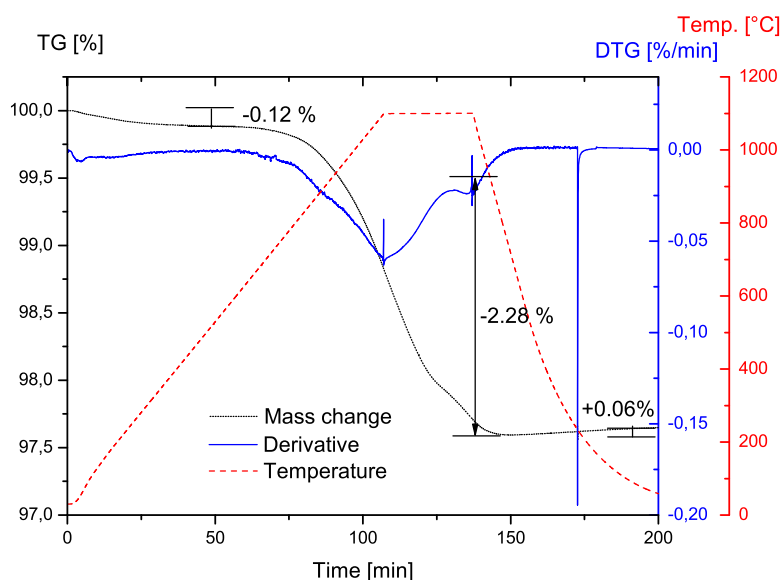

Figure 31: Thermogravimetry graph of the tungsten oxide powder. Heating rate is 30 °C/min, isothermal holding time 30 min at 1100 °C followed by cooling at an average rate of ~30 °C/min to 300 °C.

Figure 32 shows XRD patterns of the as received WO_3 and after thermal activation at 1100 °C for 30 min in Ar-10%CO atmosphere. Initially no other reflection peaks but WO3 can be observed. After exposure to the reducing atmosphere mainly lower oxide $W_{18}O_{49}$ ($WO_{2.72}$) is present in the XRD pattern. Accurate identification of further oxides is hindered by the complex peak patterns overlapping each other. The measured mass loss of 2.40 % is higher than the theoretical value of 1.93 % for reduction of WO_3 to $WO_{2.72}$. Partial reduction to lower oxides is therefore probable but cannot conclusively be confirmed by XRD.

Treatment of WO_3 in Ar-10%CO without admixed carbon shows only partial reduction and no indications of carburization. The synthesis conditions are therefore not sufficient for both reduction and carburization.
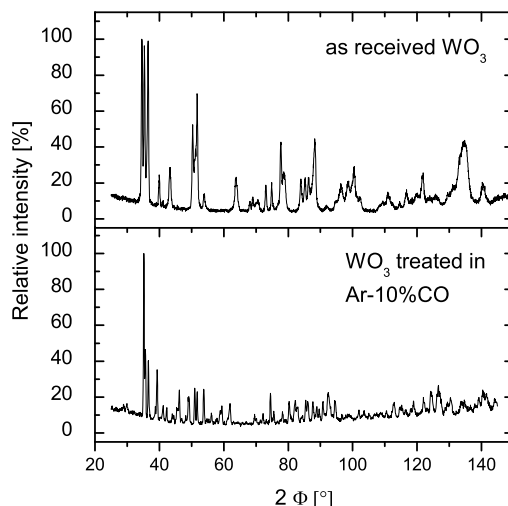
Figure 32: XRD patterns of as received tungsten oxide and after treatment in Ar-10%CO atmosphere at 1100 °C for 30 min.

Figure 33 shows the CO/CO_2 equilibrium ratios for the partial reduction steps towards complete reduction to metallic W. The corresponding ratio at the applied reduction temperature of 1100 °C for reduction to $W_{18}O_{49}$ ($WO_{2.72}$) is about 0.03, ratio for further reduction towards WO_2 is 1.1 and for the final step 2.2. The presence of mainly $W_{18}O_{49}$ suggests therefore that the average CO/CO_2 ratio in the vicinity of the reacting oxide is in the range of 0.03 to 1.1. Further reduction at the given temperature and time can therefore only be provided if the CO/CO_2 ratio is improved by efficient removal of generated CO_2 or regeneration of CO from carbon dioxide and graphite powder.
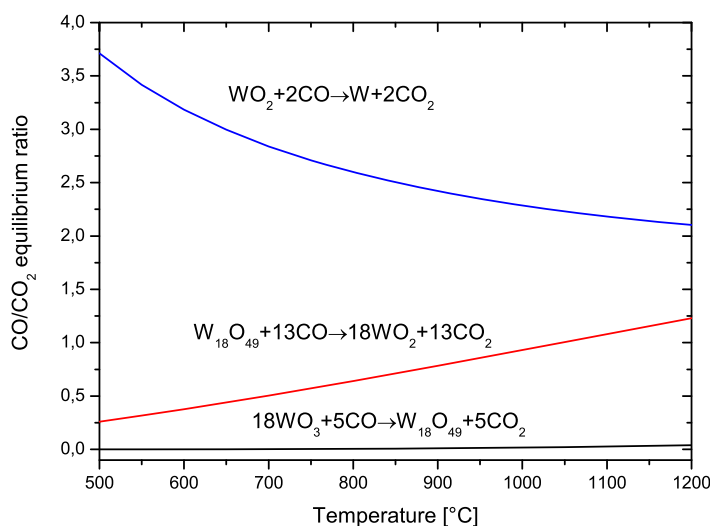

Figure 33: The equilibrium ratios of CO/CO_2 for the relevant reduction steps. Data obtained by thermochemical simulation software "HSC Chemistry" Version 7.1.

C. Reduction and Carburization by Combination of Solid Carbon with Gaseous CO

Figure 34 compares the formed phases after mechanical and thermal activation in inert Ar (as reported in chapter A) to reducing Ar-10%CO atmosphere. The combination of solid carbon in form of graphite and reducing/carburizing atmosphere yields in complete reduction. No oxide phases can be detected

after thermal activation and mass loss of 29.15 % is close to theoretical value for complete reduction of 30.02 %. Furthermore the WC/W$_2$C ratio is significantly higher as compared to powder carbon mix treated in pure Ar (compare Table 7) which indicates more beneficial synthesis conditions towards full carburization.
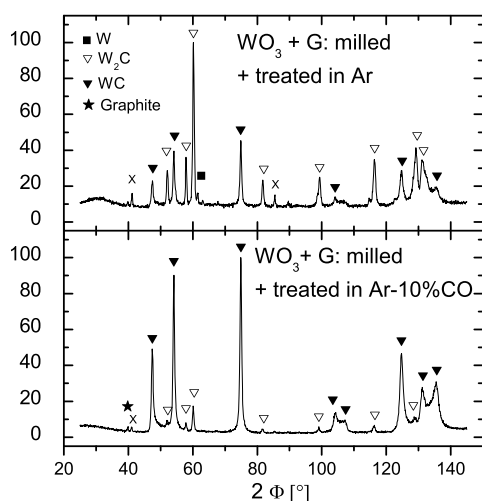

Figure 34: Comparison of XRD patterns after thermal activation of WO$_3$-graphite mixes at 1100 °C for 30 min in Ar (upper figure) and Ar-10%CO (lower) atmosphere.
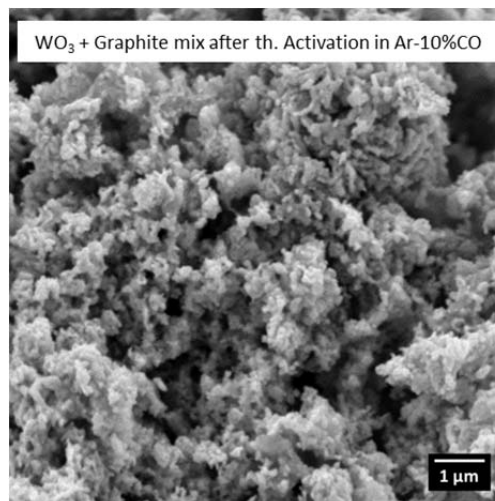

Figure 35: SEM image of WO$_3$-graphite mix thermally activated in Ar-10%CO.

Table 7: Calculated quantities of formed phases after thermal activation of WO$_3$-graphite mixes in inert Ar atmosphere as compared to Ar-10%CO atmosphere.

Phase	Content [%]	
	Ar atmosphere	Ar-10%CO atmosphere
W$_2$C	79 %	19 %
WC	19 %	81 %
X	2 %	0 %

Both the reducing ability (only partial reduction, see chapter 4.2.2 B) and the carburization effect (partial carburization, see XPS analysis in chapter 4.2.1 B) of the Ar-10%CO atmosphere at the given synthesis conditions were shown to be rather small compared to the effect of solid carbon.

Nevertheless the combination of both solid carbon and Ar-10%CO showed to have profound positive effect on the carburization yield and can only be explained by the interactions between the tungsten precursor, the solid carbon source, and the CO/CO$_2$ in the atmosphere.

In the following the differences to the case of reduction only by solid carbon as described in chapter 4.2.2 will be discussed. The initial direct solid-solid reaction via WO$_3$+C(s) $\rightarrow$ WO$_2$+CO followed by indirect reduction via WO$_3$+CO $\rightarrow$ WO$_2$ + CO$_2$ should not be influenced since diffusion of CO and CO$_2$ through the porous WO$_2$ structure is the rate determining step.

With start of stage two of the indirect reduction via WO$_2$+2CO $\rightarrow$ W+2CO$_2$ the re-generation of CO by solid carbon C(s)+CO$_2$ $\rightarrow$ 2CO becomes rate determining in case of only solid carbon present. Addition of CO through the atmosphere will hence increase the amount of available CO for reduction which increases the CO/CO$_2$ ratio. Based on this hypothesis the reduction is finished at an earlier stage. Formation of activated carbon atoms for carburization starts therefore faster which together with

enhanced CO content in the atmosphere gives a higher degree of carburization during thermal activation.

Comparison of WC crystallite sizes formed by treatment in Ar to Ar-10%CO is presented in Figure 36. WC crystallites formed are 26 nm. There seems to be no influence of the reducing/carburizing atmosphere on the crystallite size.
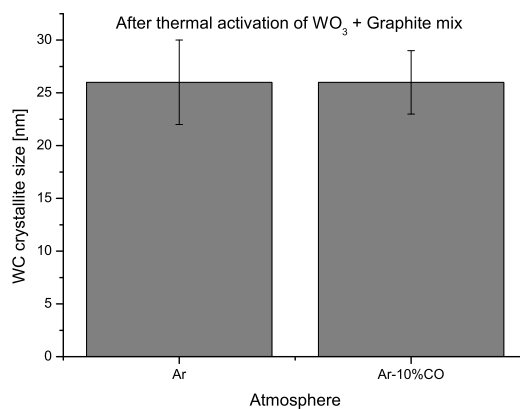

Figure 36: Resulting WC crystallite sizes of thermal activation in Ar and Ar-10%CO.

5   Conclusions

In the present study the synthesis of nanostructured WC powders has been addressed considering a process of mechanical and thermal activation of mixes containing different tungsten and carbon precursors (W-C and WO_3-C). The influence of the carbon source type in both mechanical and thermal activation stages, as well as the effect of CO containing atmospheres on the reduction/carburization processes, was investigated in order to improve the efficiency of the synthesis.

- Independently of the carbon source used, milling conditions offer efficient comminution and homogeneous mixing of W-C mixes with 1:1 mole ratio.
- Subsequent thermal activation of W-C mixes at 1100 °C causes complete carburization that can be attributed to the large contact area between the precursors.
- Comminution issues arising from the increase in the carbon content needed in mixes WO_3–C were for the most part solved by separate pre-milling of WO_3 powder.
- Thermal activation of WO_3-C mixes at 1100 ^{0}C in Ar yielded in complete reduction but incomplete carburization.
- Graphite is beneficial for initial carburization to intermediate W_2C, while carbon black promotes carburization to WC.
- Limited reducing activity of CO-containing atmosphere is observed after thermal activation of WO_3 in Ar-10%CO at 1100 ^{0}C without presence of solid carbon, where only partial reduction to intermediate oxides (mainly $W_{18}O_{49}$) was achieved.
- The carburizing capability of CO from processing atmosphere was shown based on carbon uptake seen from chemical analysis and partial formation of WC and W_2C on the powder surface, detected by XPS analysis of W powder thermally activated at 1100 ^{0}C in Ar-10%CO.
- Substantially higher efficiency of WC synthesis from WO_3-C is obtained when using CO containing atmospheres. Almost full transformation of WO_3-C mixes to WC (with only small traces of W_2C) is achieved at 1100 ^{0}C in Ar-10%CO.

6 References

[1]   G. S. Upadhyaya, *Cemented Tungsten Carbides: Production, Properties and Testing (Materials Science and Process Technology)*, 1st ed. William Andrew, 1999, p. 420.

[2]   Sandvik AB, "Sandvik Hard Metals." [Online]. Available: http://www.hardmaterials.sandvik.com/sandvik/0130/Internet/SE03459.NSF. [Accessed: 27-Jan-2014].

[3]   G. S. Upadhyaya, "Consolidation of Cemented Carbides," in *Cemented Tungsten Carbides*, 1998, pp. 89–137.

[4]   A. S. Kurlov and A. I. Gusev, *Tungsten Carbides: Structure, Properties and Application in Hardmetals (Springer Series in Materials Science)*. Springer, 2013, p. 250.

[5]   International Tungsten Industry Association, "Primary Uses of Tungsten," 2011. [Online]. Available: http://www.itia.info/tungsten-primary-uses.html. [Accessed: 04-Feb-2014].

[6]   W. Schubert, E. Lassner, and W. Böhlke, "Cemented Carbides - A Success Story," London, 2010.

[7]   Sandvik AB, "Sandvik Coromant." [Online]. Available: http://www.sandvik.coromant.com/en-gb/knowledge/materials/cutting_tool_materials/coated_cemented_carbide/pages/default.aspx. [Accessed: 16-Jun-2014].

[8]   N. J. Petch, "The cleavage strength of polycrystals," *J. Iron Steel Inst.*, no. 174, pp. 25–28, 1953.

[9]   E. O. Hall, "The Deformation and Ageing of Mild Steel: III Discussion of Results," *Proc. Phys. Soc.*, vol. 64, no. 9, pp. 747–753, 1951.

[10]   E. Lassner and W.-D. Schubert, *Tungsten: Properties, Chemistry, Technology of the Element, Alloys, and Chemical Compounds*. Springer, 1999, p. 422.

[11]   ASM and A. S. for Metals, *ASM Handbook: Volume 18: Friction, Lubrication, and Wear Technology*. ASM International, 1992, p. 942.

[12]   R. Vaûen and D. Sto, "Processing and properties of nanophase ceramics," vol. 93, 1999.

[13]   P. Maheshwari, Z. Z. Fang, and H. Y. Sohn, "Early-stage sintering densification and grain growth of nanosized WC-Co powders," *Int. J. Powder Metall. (Princeton, New Jersey)*, vol. 43, no. 2, pp. 41–47, 2007.

[14]   W.-D. Schubert, "2000 International conference on tungsten hard metals and refractory alloys," 2000.

[15]   W. D. Schubert, "Kinetics of the hydrogen reduction of tungsten oxides," *Int. J. Refract. hard Met.*, vol. 9, no. 4, pp. 178–191, 1990.

References

[16]   K. J. A. Brookes, *World Directory and Handbook of Hardmetals and Hard Materials*, 5th ed. International Carbide Data, 1992, p. 464.

[17]   R. J. Fries, J. E. Cummings, and S. A. Hoffman, "No Title," in *6th Plansee Seminar*, 1968, pp. 568–607.

[18]   T. Zheng-ji, "Study of carburization of coarse tungsten powder," *Int J Refract Met Hard Mater*, 1987.

[19]   L. V Mccarty, R. Donelson, and R. F. Hehemann, "A Diffusion Model for Tungsten Powder Carburization," vol. 18, no. June, pp. 969–974, 1987.

[20]   Y. Zhong and L. Shaw, "A study on the synthesis of nanostructured WC–10 wt% Co particles from WO3, Co3O4, and graphite," *J. Mater. Sci.*, vol. 46, no. 19, pp. 6323–6331, Oct. 2010.

[21]   J. Ma and S. G. Zhu, "Direct solid-state synthesis of tungsten carbide nanoparticles from mechanically activated tungsten oxide and graphite," *Int. J. Refract. Met. Hard Mater.*, vol. 28, no. 5, pp. 623–627, Sep. 2010.

[22]   W. Liu, X. Song, J. Zhang, G. Zhang, and X. Liu, "Thermodynamic analysis for in situ synthesis of WC–Co composite powder from metal oxides," *Mater. Chem. Phys.*, vol. 109, no. 2–3, pp. 235–240, Jun. 2007.

[23]   R. Koc and S. K. Kodambaka, "Tungsten carbide (WC) synthesis from novel precursors," *J. Eur. Ceram. Soc.*, vol. 20, no. 11, pp. 1859–1869, Oct. 2000.

[24]   F. F. . Medeiros, S. . De Oliveira, C. . De Souza, a. G. . Da Silva, U. . Gomes, and J. . De Souza, "Synthesis of tungsten carbide through gas–solid reaction at low temperatures," *Mater. Sci. Eng. A*, vol. 315, no. 1–2, pp. 58–62, Sep. 2001.

[25]   P. Scherrer, "Estimation of the size and internal structure of colloidal particles by means of röntgen.," *Nachr. Ges. Wiss. Göttingen 2*, vol. 2, pp. 96–100, 1918.

[26]   a. Patterson, "The Scherrer Formula for X-Ray Particle Size Determination," *Phys. Rev.*, vol. 56, no. 10, pp. 978–982, Nov. 1939.

[27]   J. I. Langford and A. J. C. Wilson, "Scherrer after sixty years: A survey and some new results in the determination of crystallite size," *J. Appl. Crystallogr.*, vol. 11, no. 2, pp. 102–113, Apr. 1978.

[28]   "Powder Diffraction Files (PDF-4)," *Int. Crystalography Diffr. Data*, 2012.

[29]   P. K. Gallagher, "Thermogravimetry and Thermomagnetometry," in *Handbook of Thermal Analysis and Calorimetry. Vol. 1: Principals and Practice*, vol. 1, M. E. Brown, Ed. Elsevier, 1998, pp. 225–278.

[30]   *Operating Instructions - Simultaneous TG-DTA/DSC Apparatus - STA 449 F1 Jupiter*. Selb, Germany: NETZSCH-Gerätebau GmbH, 2011.

[31]   C. D. Wagner, *Handbook of x-ray photoelectron spectroscopy: A reference book of standard data for use in x-ray photoelectron spectroscopy*. Perkin-Elmer Corporation, 1979, p. 190.

References

[32]   J. B. Lumsden and G. M. Crankovic, "X-Ray Photoelectron Spectroscopy," in *ASM Handbook: Volume 10: Materials Characterization*, 9th ed., ASM International, 1986, p. 761.

[33]   J. F. Watts and J. Wolstenholme, *An Introduction to Surface Analysis by XPS and AES*. Chichester, UK: John Wiley & Sons, Ltd, 2003.

[34]   L. Nyborg, A. Nylund, and I. Olefjord, "Thickness determination of oxide layers on spherically-shaped metal powders by ESCA," *Surf. Interface Anal.*, vol. 12, no. 2, pp. 110–114, Jul. 1988.

[35]   E. H. R. G. L. N. L. A. Raquel de Oro Calderon, "Synthesis of Nanostructured Tungsten Carbide Powders from Mechanically Activated Mixes of Tungsten Oxide with Different Carbon Sources," *Euro PM2013 Proc. - Hardmetals*, vol. 1, pp. 89–94, 2013.

[36]   C. Oikonomou, D. Nikas, E. Hryha, and L. Nyborg, "Evaluation of the thickness and roughness of homogeneous surface layers on spherical and irregular powder particles," *Surf. Interface Anal.*, no. February, p. n/a–n/a, Mar. 2014.

[37]   C. J. Powell and A. Jablonski, "NIST Electron Effective-Attenuation-Length Database." National Institute of Standards and Technology, Gaithersburg, MD, 2011.

[38]   R. J. Colton and J. W. Rabalais, "Electronic structure to tungsten and some of its borides, carbides, nitrides, and oxides by x-ray electron spectroscopy," *Inorg. Chem.*, vol. 15, no. 1, pp. 236–238, Jan. 1976.

[39]   B. Kim, J. Chen, J. Erskine, W. Mei, and C. Wei, "Surface and bulk photoelectron diffraction from W(110) 4f core levels.," *Phys. Rev. B. Condens. Matter*, vol. 48, no. 7, pp. 4735–4740, Aug. 1993.

[40]   K. Håkansson, H. Johansson, and L. Johansson, "High-resolution core-level study of hexagonal WC(0001).," *Phys. Rev. B. Condens. Matter*, vol. 49, no. 3, pp. 2035–2039, Jan. 1994.

[41]   D. Mueller, "A synchrotron radiation study of BaO films on W(001) and their interaction with H2O, CO2, and O2," *J. Vac. Sci. Technol. A Vacuum, Surfaces, Film.*, vol. 6, no. 3, p. 1067, May 1988.

[42]   T. Aizawa, S. Hishita, T. Tanaka, and S. Otani, "Surface reconstruction of $W_2C(0001)$.," *J. Phys. Condens. Matter*, vol. 23, no. 30, p. 305007, Aug. 2011.

[43]   J. Luthin and C. Linsmeier, "Carbon films and carbide formation on tungsten," *Surf. Sci.*, vol. 454–456, pp. 78–82, May 2000.

[44]   D. S. Venables and M. E. Brown, "Reduction of tungsten oxides with carbon . Part 1 : Thermal analyses," *Thermochim. Acta*, vol. 282/283, pp. 251–264, 1996.

[45]   D. S. Venables and M. E. Brown, "Reduction of tungsten oxides with carbon . Part 2 . Tube furnace experiments," *Thermochim. Acta*, vol. 282/283, pp. 265–276, 1996.

[46]   D. S. Venables and M. E. Brown, "Reduction of tungsten oxides with carbon monoxide," *Thermochim. Acta*, vol. 291, pp. 131–140, 1997.

References

[47]   E. J. Rees, C. D. a. Brady, and G. T. Burstein, "Solid-state synthesis of tungsten carbide from tungsten oxide and carbon, and its catalysis by nickel," *Mater. Lett.*, vol. 62, no. 1, pp. 1–3, Jan. 2008.

[48]   A. K. Basu and F. R. Sale, "A Morphological Study of the Carburization /," vol. 9, no. December, 1978.